

POLITECNICO DI TORINO

Collegio di Ingegneria Meccanica, Aerospaziale, dell'Autoveicolo

Master of Science Course in Mechanical Engineering

Master of Science Thesis

Modelling and simulation of a Latent Heat Thermal Energy Storage



**Politecnico
di Torino**

Tutors

Prof. Vittorio Verda

Ing. Martina Capone

Candidate

Alberto Micheluz

July 2024

Abstract

The transformation of the global energy system in line with the Paris Agreement requires rapid uptake of renewables throughout all kinds of energy use. As a result the low-carbon heating technologies are growing, but the energy demand is still mostly met by fossil fuels. In order to accelerate a wider transition to renewable energy solutions in the heating sector, thermal energy storage (TES) technologies can be used. TES help to integrate high shares of renewable energy in power generation, industry and buildings. Several energy storage options exist now, but the one that has gained increasing attention and is topic of interest in this thesis is the latent heat thermal energy storage (LHTES) because it offers considerably higher energy density at a nearly constant temperature level if compared to sensible storage systems. These features are particularly interesting in the urban context, where limited installation space is required for TES units. Despite its considerable potential, market deployment has only been achieved by a restricted number of commercial devices. This may be related to two principal conditions: firstly the lack of accurate and at the same time fast models, which would facilitate LHTES integration in energy systems; secondly the limited knowledge on how full scale LHTES devices interact with the heating systems in which they are incorporated.

This thesis tries to overcome the former problematic by implementing a fast and accurate model for system-level simulations of shell-and-tube latent heat storage units. Such a model is entirely based on a-priori known physical and geometrical parameters. Different fins geometries are analysed while considering also different materials for the phase change material (PCM) used to store the thermal energy. In order to achieve a better accuracy for the model with respect to a more realistic three dimensional one, the effect of such variables are considered thanks to the definition of a few parameters, which are mainly focused on the geometrical properties of the fins as well as the thermal properties of the selected PCM.

Contents

List of Figures	iv
List of Tables	vi
Nomenclature	vii
1 Introduction	1
1.1 Context	1
1.2 Objectives	2
1.3 Outline of the thesis	3
2 State of the art on LHTES	5
2.1 Overview on thermal energy storage	6
2.2 Phase change materials	8
2.2.1 PCMs properties	8
2.2.2 PCMs classification	11
2.2.3 Melting temperature range and application area	17
2.3 PCM containers for LHTES	18
2.4 LHTES fins design approaches	20
2.5 State of the art on LHTES modelling	27
2.5.1 Apparent heat capacity method	30
2.5.2 Effective capacity method	31
2.5.3 Source based method	31
2.5.4 Enthalpy method	32
2.6 LHTES system integration	33
3 Three-dimensional LHTES models	35
3.1 Brief overview on COMSOL Multiphysics	35

3.2	Geometry and materials	36
3.2.1	PCM design	36
3.2.2	Fins design	38
3.3	Numerical model	42
3.3.1	PCM's specific heat capacity model	42
3.3.2	Physics, mesh and study	43
3.3.3	Post-processing	45
4	One-dimensional LHTES model	52
4.1	Brief overview on MATLAB	53
4.2	Methodology	53
4.3	Model for the HTF domain	54
4.4	Thermal power characteristic curves for LHTES heat transfer rate	56
4.4.1	Derivation of the time constant τ_0	59
4.4.2	Derivation of the shape factor β	61
4.5	Model solution algorithm	63
5	Models comparison	67
5.1	First comparison	68
5.2	Correcting parameters	72
5.3	Final comparison	75
6	Conclusions	82
6.1	Research contributions	82
6.2	Limitations and future perspectives	83
	References	85

List of Figures

2.1	Classification of PCMs	12
2.2	Different types of PCMs and their latent heat of fusion as function of the melting temperature [25]	12
2.3	Configuration classification of commonly used PCM containers [5]	20
2.4	Schematic diagram of uniform and non-uniform fin height [64]	22
2.5	Comparison of a circular fin, helical fin and longitudinal fin LHTES unit [56, 67]	26
2.6	(a) Three dimensional view of Snowflake shaped fin [70], (b) 3D design visualization of a sectioned finned unit using topology optimization [72]	27
2.7	Solid-liquid interface during the PCM phase change process [7]	28
2.8	Enthalpy as a function of temperature for (a) isothermal phase change; (b) nonisothermal phase change [74]	33
3.1	(a) Longitudinal fins LHTES domain; (b) Mesh of the longitudinal fins LHTES domain	41
3.2	(a) Circular fins LHTES domain; (b) Mesh of the circular fins LHTES domain	42
3.3	Equivalent specific heat for the PCM [J/(kgK)]	43
3.4	Average PCM temperature [K]	45
3.5	Average HTF outlet temperature [K]	46
3.6	Average heat flux [W/m ²]	46
3.7	Average PCM temperature [K]	47
3.8	Average HTF outlet temperature [K]	47
3.9	Average heat flux [W/m ²]	48
3.10	Average PCM temperature [K]	48
3.11	Average HTF outlet temperature [K]	49
3.12	Average heat flux [W/m ²]	49

3.13	Average PCM temperature [K]	50
3.14	Average HTF outlet temperature [K]	50
3.15	Average heat flux [W/m ²]	51
4.1	Example of normalized discharge energy over time	57
4.2	Effect of different β values on the normalized discharged energy	62
4.3	Linearization of the heat rate exchanged at the contact wall	64
5.1	Paraffin, longitudinal fins	68
5.2	Paraffin, circular fins	69
5.3	Salt hydrate, longitudinal fins	69
5.4	Salt hydrate, circular fins	70
5.5	Paraffin, longitudinal fins	70
5.6	Paraffin, circular fins	71
5.7	Salt hydrate, longitudinal fins	71
5.8	Salt hydrate, circular fins	72
5.9	Paraffin PCM average temperature	73
5.10	Salt hydrate PCM average temperature	74
5.11	Paraffin, longitudinal fins	76
5.12	Paraffin, circular fins	77
5.13	Salt hydrate, longitudinal fins	77
5.14	Salt hydrate, circular fins	78
5.15	Paraffin, longitudinal fins	78
5.16	Paraffin, circular fins	79
5.17	Salt hydrate, longitudinal fins	79
5.18	Salt hydrate, circular fins	80

List of Tables

2.1	Different PCMs characteristics and applications (adopted from [7, 31])	18
3.1	Paraffin thermal and physical properties (adopted from [7])	37
3.2	Salt hydrate thermal and physical properties	37
3.3	Pipe geometrical characteristics	39
3.4	Copper thermo-physical properties	39
3.5	Aluminum thermo-physical properties	40
3.6	Longitudinal fins geometrical characteristics	40
3.7	Circular fins geometrical characteristics	40
5.1	HTF outlet temperature average relative error	80
5.2	SOC maximum error	81

Nomenclature

Acronyms / Abbreviations

DH District Heating

ESS Energy Storage System

HCM High Conducting Material

HP Heat Pump

HTF Heat Transfer Fluid

LHTES Latent Heat Thermal Storage

Nu Nusselt non-dimensional number

PCM Phase Change Material

Pr Prandtl non-dimensional number

Re Reynolds non-dimensional number

St Stefan non-dimensional number

TCS Thermo-Chemical heat Storage

TES Thermal Energy Storage

TRL Technology Readiness Level

Subscripts

0 initial condition

<i>avg</i>	average
<i>dis</i>	discharge
<i>in</i>	inlet
<i>j</i>	j-th discretized element
<i>l</i>	liquid
<i>ls</i>	solid-liquid interface
<i>n</i>	normalized
<i>out</i>	outlet
<i>pc</i>	phase change point
<i>ref</i>	arbitrary reference condition
<i>s</i>	solid
<i>tot</i>	total
<i>wall</i>	contact wall between HTF pipe and PCM-HCM assembly

Greek Symbols

α	Thermal diffusivity [m^2/s]
β	Shape factor [-]
Δ	Difference
γ	Fin shape factor [-]
ρ	Density [kg/m^3]
τ_0	Time scale factor [s]

Roman Symbols

Δh_{lat}	Latent heat specific content [J/kg]
A	Matrix for the 1D discretized pure advection problem

A_{lat}	Lateral surface of each pipe discretized volume [m ²]
A_{pipe}	Pipe external surface [m ²]
b	Right-end side vector for the 1D discretized pure advection problem
c_p	Specific heat capacity [J/(kgK)]
d_i	Pipe inner diameter [m]
E	Energy [J]
G	Flow rate [l/h or kg/s]
h	Enthalpy [J/kg]
h_{conv}	Convective heat transfer coefficient [W/(m ² K)]
k	Thermal conductivity [W/(mK)]
l_c	PCM characteristic length around each pipe [m]
M	Mass [kg]
q	Heat rate [W or W/m]
q'''	Volumetric heat generation [W/m ³]
SOC	State of charge [-]
T	Temperature [°C or K]
u	Fluid velocity [m/s]
V	Volume [m ³]
z	Longitudinal axis

Superscripts

n	n-th timestep
-----	---------------

Chapter 1

Introduction

1.1 Context

The surge in global energy demand, driven by the population growth, escalating climate concerns and current geopolitical realities, necessitates a profound shift in how we generate and utilize energy. Nevertheless, according to the IEA's November 2023 Oil Market Report, global oil demand was forecast to increase by 2.4% in 2023 [1]. In tackling this crucial issue, relying solely on renewable energy technologies proves inadequate help, due to the intrinsic unpredictability of renewable energy sources. Within this framework, the pivotal component for facilitating the shift from a fossil fuel-dependent society (where energy accessibility is assured) to one reliant on renewables (which seeks energy on demand) lies in energy storage solutions.

Energy efficiency is currently seeing a strong global focus among policy makers in recognition of its important role in enhancing energy security and affordability, and in accelerating clean energy transitions. Since the start of the energy crisis in early 2022 there has been a major escalation in action, with countries representing 70% of global energy demand introducing or significantly strengthening efficiency policy packages [1].

In the production of CO_2 emissions, a great contribution comes from the building sector, where the operations of buildings account for 30% of global final energy consumption and 26% of global energy-related emissions [2]. Most of the energy consumption in buildings is related to space and water heating. Nearly two thirds of heating energy use still rely on fossil fuels [3].

The role of efficient and low-carbon heating technologies continues to grow, but fossil fuels still meet over 60% of heating energy demand [3]. That's why thermal energy storage (TES) represents a very important resource in contrasting fossil fuels consumption. It allows far greater reliance on variable renewable sources, such as solar and wind power. TES reduces the need for costly grid reinforcements, helps to balance seasonal demand and supports the shift to a predominantly renewable-based energy system [4].

When looking at the available TES options, those based on latent heat have gained an important spot in the last years. Innovation is still needed to increase the commercial readiness of such technologies. Latent heat thermal energy storage (LHTES) technologies rely on the use of phase change materials (PCMs), which are characterised by high energy density and allow charge/discharge cycles at a nearly constant temperature, which corresponds to the phase transition temperature of the PCM [5]. The first characteristic is especially important for use in residential settings, which typically have limited installation space for TES devices.

1.2 Objectives

The body of literature concerning LHTES technologies is quite wide. Indeed, the properties of PCMs are mostly known and tested, also guidelines for the creation of effective LHTES devices exist. The main reason why these TES solutions are not yet so popular is because the Technology Readiness Level (TRL) of only a few of these PCM systems has reached at least the first step of the deployment phase (level 7) [6]. Looking at the current situation, what are needed are improvements to well-identified solutions that could fully exploit the huge potential of LHTES technologies and overcome the present limits.

The enhancement of the heat transfer inside LHTES units and the optimization of PCM properties are the main problems that have been analysed in the research field, but the integration of LHTES devices in heating systems is a topic that still needs development, from the point of view of the optimal sizing and the optimal operation. Indeed, just the PhD thesis developed by A. Colangelo [7] is discussing such topic. Multiple reasons limit the spread of these devices, but the main reason one could suggest is the lack of computationally fast and accurate mathematical models facilitating

the incorporation of latent heat storage units into energy system simulation environments [7]. In order to overcome these gaps, this thesis starts from the available fast one-dimensional model, developed by A. Colangelo [7], for the simulation of a few LHTES shell-and-tube heat exchangers given their dimensional and thermo-physical properties. Differently from the PhD thesis [7], multiple fins design and phase change materials are here evaluated. A few geometrical and thermal parameters are evaluated in order to achieve a better accuracy and matching with the three-dimensional model simulation's results.

1.3 Outline of the thesis

What follows is a general overview of each chapter.

Chapter 2 outlines the state of the art on Latent Heat Thermal Energy Storage (LHTES) technologies. This chapter gives the context needed to fully understand the behaviour and typical properties of PCMs and LHTES in general. A background concerning the different PCMs thermal and physical properties as well as the LHTES design approaches is presented.

Chapter 3 describes in detail the three-dimensional LHTES models that are used as a reference for the one-dimensional ones. Here the geometrical and thermo-physical properties of the LHTES are listed and displayed. The simulations' steps and requirements are clearly and comprehensively explained, like the used mesh, the different boundary and initial conditions of the model.

Chapter 4 explains in detail the developed one-dimensional dynamic model to simulate the behaviour of a LHTES shell-and-tube heat exchanger. This model requests a very low computational effort while keeping a very good accuracy. Here are also fully explained the essential starting hypotheses and boundary conditions. The proposed modelling approach links a one-dimensional pure advection problem for the LHTES with a mathematical expression for the time dependent heat transfer rate released by the PCM and high conductive material (HCM), which is called thermal power characteristic curve.

Chapter 5 displays the results obtained in the previous chapters. The comparison of the one-dimensional model simulation results and the ones of

the three-dimensional model simulation is performed.

Eventually, Chapter 6 draws the conclusions by analysing the obtained results and limitations of this work and identifies possible future perspectives.

Chapter 2

State of the art on LHTES

In this chapter the available scientific literature about the most relevant aspects on thermal energy storages based on latent heat is summarised.

Section 2.1 sets the context in which LHTES technologies should be studied.

Section 2.2 summarises the main thermo-physical properties of phase change materials (PCMs) and a classification of the main typologies of PCMs is described in detail.

Section 2.3 describes the main solutions for PCM containers in order to realise the LHTES heat exchanger.

Section 2.4 lists the most popular fins design approaches when dealing with LHTES shell-and-tube heat exchangers in order to deal with the PCM low thermal conductivity.

Section 2.5 provides an overview on the main modelling approaches for representing the thermal behaviour of LHTES systems.

Section 2.6 presents some LHTES units that have been integrated into different heating systems.

2.1 Overview on thermal energy storage

A prevalent issue encountered in most renewable energy production systems revolves around the mismatch between the duration of thermal energy availability and its actual utilization [8]. This circumstance highlights the necessity for an efficient approach to store surplus heat for future utilization. Latent heat thermal energy storage is one of the most efficient ways of storing thermal energy through which the disparity between energy production or availability and consumption can be corrected, thus avoiding wastage and increasing the process efficiency [8]. Even when considering urban district heating systems, in the first hours of the morning the sharp increase in heating demand leads to greater greenhouse gas emissions at the facility level [9]. It is important to understand that the path towards decarbonisation of the heating sector needs an intensive introduction of auxiliary systems like TES devices, particularly LHTES ones.

Before diving into LHTES solutions, let's see which are the main energy storage system (ESS) solutions available. We can summarise them as: mechanical, electrochemical, chemical and thermal storage [10]. Mechanical energy manifests as potential energy or kinetic energy. Mechanical energy storage is generally used at large scale for grid applications. Its main advantages are the following [10]: it can be stored easily and for long periods of time; it is very flexible, i.e. it can be easily converted into and from other energy forms. Among them, the pumped hydro storage, compressed air energy storage systems and flywheel energy storage system are the most well-known. Most of these technologies, with some exceptions, can provide exceptionally high energy storage and power densities, making them suitable for extensive and prolonged electricity storage. Technologies capable of multigeneration can also play a crucial role in sector coupling, enhancing their ability to support the integration of variable renewable energy sources like wind turbines [11]. The second group of ESS are electrochemical energy storage systems, which consist of all rechargeable battery energy storage and flow battery. They are one of the oldest, and consequently, most mature technologies available. The chemical energy contained in the active materials is converted into electrical energy by means of electrochemical oxidation–reduction reaction [10]. Differently from the previous solution, these devices have a wide range of energy density, hence they can be deployed at different scales, from small residential applications to utility scale. Its main advantages are the following [10]: it

has high efficiency of 70–80% and a negligible amount of harmful substance emission; they require very little maintenance. Such storage systems are essentially constituted by numerous types of batteries, like lead acid, lithium based (Li metal, Li-ion, Lithium polymer), metal air, nickel based and flow batteries. Batteries offer the highest efficiencies among all electricity storage methods [11]. They are not limited by geographical or sizing constraints, allowing for deployment near the application site and easy scalability. However, batteries do have notable drawbacks, including high costs, a relatively short lifespan due to a limited number of charge/discharge cycles, and low storage density [11]. The next family of ESS are chemical energy storage systems, where energy can be stored for a long time in the form of chemical bonds of molecules [10]. The reactants and products of chemical reactions are entirely different. Thus, energy can be converted from one chemical form to another [10].

For what concerns thermal energy storage systems, these can be classified in [12]: sensible thermal energy storage (TES or STES), latent heat thermal energy storage (LHTES) and thermo-chemical heat storage (TCS). STES involves heating a material, without actually causing a phase change in it. Thermal energy is accumulated as a result of increasing the temperature of the storage medium. The amount of energy stored Q may be represented by the following expression [13]:

$$Q = \int_{T_i}^{T_f} mc_p dT \quad (2.1)$$

It depends on the specific heat c_p , the temperature change dT and the amount of material m . STES systems can be classified on the basis of the storage material as liquid media sensible storage (e.g. water, oil) or solid media sensible storage (e.g. rocks, metals) [12]. When dealing with LHTES the material is heated up/cooled down until it experiences a phase change, which can be from solid to liquid (and vice-versa) or from liquid to gas (and vice-versa); when the material reaches its phase change temperature it absorbs/releases a large amount of heat in order to carry out the transformation and in this manner the energy is stored/released. The storage capacity of a LHTES system can be represented by the following expression [13]:

$$Q = \int_{T_i}^{T_{pc}} mc_p dT + m\Delta h_{pc} + \int_{T_{pc}}^{T_f} mc_p dT \quad (2.2)$$

Where T_{pc} is the phase change temperature and Δh_{pc} is the latent heat capacity. Materials used for latent heat thermal energy storage are known as phase change materials (PCMs). The PCM may undergo solid–solid, solid–liquid and liquid–gas phase transformations. The first scenario is adopted when we want to prevent the liquid from leaking without having the capsules decreasing the energy density of the system and increase the cost of production [14]. Transformations from liquid to gas have the highest latent heat of phase change; however, the enormous changes in the volume of the storage material associated with the evaporation make the storage complex and highly impractical [12]. Looking at the last possibility, the change from solid to liquid phase is the transformation that has been most widely studied and used in LHTES applications; it has a lower latent heat compared with the liquid–gas phase change, but it does not present such a serious problem regarding volumetric expansion, which is generally in the order of an increase of 10% or less relative to the original volume [12]. If we talk about thermochemical heat storage instead it consists in the use of reversible endothermic chemical reactions [10]. The chemical heat is the heat necessary to dissociate or break joints in a chemical compound; nearly all of this energy will be retrieved later when a synthesis reaction takes place. This solution presents multiple advantages, but the development of reversible thermochemical reactions is at a very early stage [15]. Instead, the knowledge of latent storage technologies is more advanced and as a consequence their Technology Readiness Level (TRL) is closer to market maturity [7].

2.2 Phase change materials

2.2.1 PCMs properties

As mentioned in the previous section, phase change materials (PCMs) are industrial products that experience a phase transition, usually between the solid and the liquid state. There are many important properties to consider for a viable PCM, however as highlighted in Eq. 2.2, in order to maximise heat storage capacity, the following properties must be wisely selected:

- Latent heat of solidification/fusion Δh_{pc} ;
- Density ρ ;

- Specific heat capacity c_p .

A special focus on density is important, since the PCM volume change between solid and liquid phase should be kept minimum. In fact, the PCM container is usually oversized to fit in the maximum volume during the liquid phase, so that stresses can be avoided [16].

Other important properties which should be included are: thermal conductivity, stability, cyclability, phase segregation, hysteresis, supercooling, containment, cost, and safety.

Thermal conductivity specifies the conduction of heat in the material. If thermal conductivity is too small, it will be difficult to extract energy from the PCM, or charge it, in a reasonable amount of time [17]. The homogeneity of the temperature distribution within the material is highly influenced by it. The thermal diffusivity of PCMs is generally mediocre, due to the combination of low thermal conductivity (often in the range 0.2-0.5W/(mK)) and high specific latent heat capacity [7]. Several solutions are available in order to increase the thermal conductivity of a LHTES system and they often consist in one of the following [18]:

- Fins: they are a simple, economical, and most widely used technique for heat transfer enhancement. However, it results in reduced energy storage capacity;
- Nanoparticle addition: dispersion of nanoparticles (most of them are metallic) into the PCM has been studied widely by researchers as a method to enhance melting/solidification rates, but also to reduce supercooling by creating nucleating sites to initiate solidification. However, the addition of nanoparticles compromises the overall thermal storage capacity and enhances the dynamic viscosity of the composite, which inhibits the effect of natural convection [19];
- Encapsulation: it involves enclosing the PCM within a coating made of non-reactive, stable polymers or containers, forming a capsule that can be spherical, oval, or irregular in shape. This technique can enhance the thermal conductivity, thermal stability, and supercooling properties of the PCM, as well as prevent leakage and reduce corrosion of the containment material [20]. Despite its high heat transfer, reduced leakage,

and decreased corrosion, its complex preparation method, high production cost, and potential for leakage over many thermal cycles limit its widespread acceptance compared to other enhancement methods [21];

- Porous matrix: infiltrating the PCM into the porous sites of matrices to form shape stable PCM is an effective alternative to the costly encapsulation methods [21]. This approach has been widely studied to improve thermal conductivity, supercooling, leakage, and corrosion issues associated with PCM [22]. Several porous matrices have been investigated as matrices such as porous silica metal foams and expanded graphite.

It is important for the PCM (and its container) to be stable for any long-term application (over thousands of cycles). In order to be compatible with the wanted application, the material should not degrade over time, should not react with the ambient air or moisture, and should not degrade its containment vessel [17]. Over its lifetime a few properties must be constant, i.e. it should not exhibit a notable decrease in latent heat or change in transition temperature. Furthermore, repeated melting and crystallization should not degrade or otherwise alter the material [17].

Among the most important limits to the cyclability of PCMs, separation into different phases certainly must be considered. This degradation is often seen in multi-component PCMs in which the components differ remarkably in density. In this situation, gravity could cause one component to separate from the other(s), altering the melting point of the system [17]. The enhancement of segregation of phases can happen over many cycles and lead to a gradual but remarkable decrease in performance [23].

If PCMs show different behaviour during heating and cooling processes, it means that hysteresis occurs in the material. This phenomenon leads to different transition temperatures and latent heat capacities between the solidification and melting processes [7]. The slow crystal formation during solidification is the usual cause of hysteresis. Solutions to overcome this drawback are similar to those analysed for mitigating the phase segregation phenomenon, as both problems are linked to the heat transfer rate [7].

Another very important drawback of some otherwise promising PCMs is supercooling (also known as subcooling). Supercooling is the persistence of the high-temperature phase below its transition temperature [17]. Below

the transition temperature, the high-temperature phase is metastable, but could supercool by at least 100 K before eventually transitioning to the stable phase [17]. The supercooling degree is the temperature difference between the liquidus temperature of melting and the crystallization temperature [24]. If the system supercools below the application's minimum temperature, the stored latent heat will be lost and, after the initial heating, the PCM will function solely as a sensible heat storage material [17].

The PCM also has to be compatible with its container. The PCM should not corrode, degrade, or soften/dissolve the material containing it [17]. Furthermore, the containment vessel must be able to hold the PCM's liquid phase without leaking its contents.

To realize widespread, cost-effective utilization of latent heat storage, it is essential for PCMs to be easily accessible and affordable. Even if a material presents great stability and superior thermal characteristics, it may not be suitable as a PCM if its price is too much expensive. Ideally, a PCM should also be safe for household applications, characterized by low toxicity, non-violent reactivity, and minimal fire hazard [17].

2.2.2 PCMs classification

When selecting the phase change material for the specific application, other than the physical and chemical properties previously mentioned, one should also consider the phase change temperature of the PCM itself, which has to be within the practical range of application. Regarding the technical requirements, PCMs can be categorized as [7]: organic, which mainly consist of paraffins, fatty acids alcohols and glycols; inorganic, that mainly consist of salt hydrates and metallic alloys; eutectic mixtures, which consist of different constituents and can be organic-organic, organic-inorganic or inorganic-inorganic. In Figure 2.1 are summarized the main solutions.

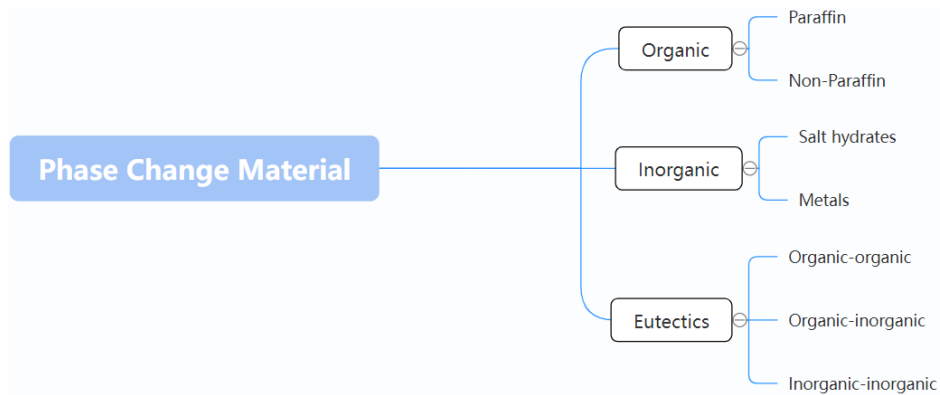


Figure 2.1: Classification of PCMs

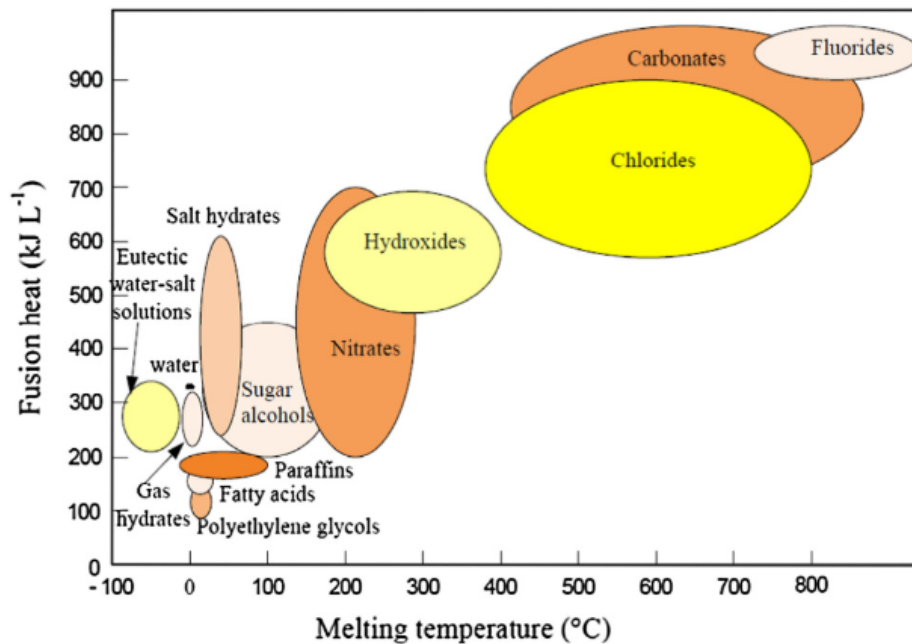


Figure 2.2: Different types of PCMs and their latent heat of fusion as function of the melting temperature [25]

As can be seen in Figure 2.2, the melting temperature and the transformation energy are not independent. A sort of correlation between the melting temperature and the specific enthalpy of phase transformation is shown in

the diagram. PCMs with a high melting temperature (like salts) have a high energy density, whereas the ones with a low melting temperature can only retain a limited amount of latent heat throughout the phase transition [7].

Since no single material possesses all the necessary properties to serve as an ideal thermal storage medium, it is essential to use available materials and compensate for any deficiencies in their physical properties through effective system design. As a general trend, inorganic PCMs have almost double volumetric latent heat storage capacity ($250 - 400 \text{ kg/dm}^3$) than the organic ones ($128 - 200 \text{ kg/dm}^3$) [26]. Due to their distinct thermal and chemical characteristics, the properties of each subgroup, which affects the design of latent heat thermal energy storage systems using PCMs of that subgroup, are discussed in detail below.

Organic PCMs

Organic materials can be classified as paraffin and non-paraffins [26]. Organic materials include: congruent melting, which means that the materials melt and freeze repeatedly without phase segregation and consequent degradation of their latent heat of fusion; self nucleation, which means that they crystallize with little or no supercooling; usually non-corrosiveness. For these reasons they are the most adopted PCMs in commercial applications. However, they have lower density than inorganic PCMs and are flammable (above 200°C) [7]. Furthermore, they are characterised by low thermal conductivity ($\simeq 0.2 \text{ W/(mK)}$), leading to reduced heat diffusion and storage capability [7]. Additionally, paraffin materials have high volume variations during phase transition, which may not be compatible with plastic containers [7].

- Paraffins: the paraffin wax is a mixture of almost entirely straight chain alkanes $\text{CH}_3 - (\text{CH}_2) - \text{CH}_3$. A large amount of latent heat is released by the crystallization of the $(\text{CH}_3) -$ chain [26]. The melting point and latent heat of fusion both rise as the chain length increases [26]. Paraffin is an appropriate choice for heat of fusion storage materials because it is available across a broad temperature spectrum. However, for economic reasons, only technical grade paraffins are generally employed as phase change materials (PCMs) in latent heat storage systems. Paraffin is safe, reliable, predictable, non corrosive and less expensive. Below 500°C they are chemically inert and stable, they also show little volume changes on melting and have low vapor pressure in the melt form [26].

Because of these properties, systems that adopt paraffins as PCM usually have very long freeze–melt cycles. As the number of carbon atoms increases, the melting point of alkane increases [26]. These materials present multiple advantageous characteristics such as congruent melting and good nucleating properties, but they show some unwanted properties such as: (i) low thermal conductivity, (ii) non-compatible with the plastic container and (iii) moderately flammable [26]. These undesirable effects can be partially mitigated by making small modifications to the wax and the storage unit.

- Non-paraffins: the non-paraffin organics are the most diverse group of phase change materials, each possessing unique properties, unlike the paraffins, which have very similar characteristics [26]. Some researchers have conducted an extensive survey of organic materials and identified a number of esters, fatty acids, alcohol's and glycol's suitable for energy storage [27]. These are further subgrouped as fatty acids and other non-paraffin organic. These materials are flammable and should be kept away from extremely high temperatures, open flames, and oxidizing agents. The phase change temperature and latent heat of saturated fatty acids increase as the carbon chain length grows. Additionally, the use of fatty acids as PCMs is affected by their other physical and thermal properties, including density, specific heat, and thermal conductivity [28]. Some of the most interesting features of these organic materials are: (i) high heat of fusion, (ii) inflammability, (iii) low thermal conductivity, (iv) low flash points, (v) varying level of toxicity, and (vi) instability at high temperatures [26]. Fatty acids possess high heat of fusion values similar to those of paraffin. They also exhibit consistent melting and freezing behavior and solidify without supercooling [29]. Fatty acids are described by the general formula $CH_3(CH_2)_{2n} \cdot COOH$ and hence qualify as good PCMs. However their cost should be considered as well, which is 2–2.5 times greater than that of technical grade paraffin's [26]. This clearly represents one of the main drawbacks of this family of PCMs. They are also slightly corrosive.

Inorganic PCMs

Inorganic materials are classified as salt hydrate and metallics. These PCMs have the advantage of not supercooling appreciably and also their

heat of fusion does not degrade with cycling [26].

- Salt hydrates: they may be considered as alloys of inorganic salts and water forming a typical crystalline solid whose general formula is $AB \cdot nH_2O$ [26]. The change from solid to liquid in salt hydrates is essentially a dehydration or rehydration of the salt, though thermodynamically it appears similar to melting or freezing. When the melting point is reached, the hydrate crystals breakup into anhydrous salt and water, or into a lower hydrate and water [26]. A common issue with many salt hydrates is incongruent melting, which occurs because the amount of water released during crystallization is insufficient to dissolve all the solid phase. As a result, the lower hydrate (or anhydrous salt) settles at the bottom of the container due to its higher density [26]. Another problem that characterises most salt hydrates is poor nucleating properties, resulting in supercooling of the liquid before crystallization begins [26]. One way to address this issue is by adding a nucleating agent, which supplies the nuclei needed for crystal formation. Alternatively, retaining some crystals in a small, cool area can also serve as nuclei for the process [26]. Salt hydrates represent a crucial category of PCMs that have been thoroughly investigated for their application in latent heat thermal energy storage systems. The most appealing properties of salt hydrates are: (i) high latent heat of fusion per unit volume, (ii) relatively high thermal conductivity (almost double of the paraffin's), and (iii) small volume changes on melting [26]. They also are not very corrosive, compatible with plastics and only slightly toxic. Many salt hydrates are sufficiently cheap for the use in TES [26]. For the relatively low temperatures in building applications, corrosion can be avoided by using appropriate heat exchanger materials like plastics. However, a drawback is that plastics have lower thermal conductivity compared to metals, leading to lower heat transfer rates [30]. Three types of behaviour of the melted salts can be classified: congruent, incongruent and semi-congruent melting.

- Congruent melting: the anhydrous salt is completely soluble in its water of hydration at the melting temperature [26];
- Incongruent melting: the salt is not entirely soluble in its water of hydration at the melting point [26];
- Semi-congruent melting: it involves the equilibrium phase tran-

sition where the composition of the liquid and solid phases differ due to the conversion of the hydrate into a less hydrated material through water loss [26].

Incongruent melting is the main problem related to salt hydrates when using them as PCMs [26]. Since n moles of water of hydration are insufficient to dissolve one mole of salt, the resulting solution becomes supersaturated at the melting temperature. The denser solid salt settles at the bottom of the container, preventing it from recombining with water during freezing. Consequently, the melting–freezing process of the salt hydrate becomes progressively less effective with each charge–discharge cycle [26]. Supercooling is another important problem common to salt hydrates. At the fusion temperature, the nucleation rate is typically very low. To attain a reasonable nucleation rate, the solution has to be supercooled, causing energy to be discharged at a much lower temperature instead of the fusion temperature [26].

- **Metallics:** they are further subgrouped as low melting metals and metal eutectics [26]. These metallics have not been seriously considered for PCM technology due to their weight drawbacks. Nevertheless, when volume is a critical factor, they become promising candidates because of their high heat of fusion per unit volume [26]. A major difference between the metallics and other PCMs is their high thermal conductivity. Some of the most remarkable features of these materials are: (i) low heat of fusion per unit weight (ii) high heat of fusion per unit volume, (iii) high thermal conductivity, (iv) low specific heat and (v) relatively low vapor pressure [26].

Eutectics PCMs

A eutectic is a composition with the lowest melting point among a mixture of two or more components, each of which melts and freezes congruently, forming a blend of component crystals during crystallization [26]. Eutectics almost always melt and freeze without segregation because they form a close mixture of crystals, providing little chance for the components to separate [26]. On melting, both components liquefy simultaneously (separation is unlikely). However, their application in building systems is very limited and there are only a few studies available in the literature that report their thermo-physical properties [7].

2.2.3 Melting temperature range and application area

For any application the selection of an appropriate PCM requires the PCM to have its melting temperature within the practical range of application. Several application areas have been proposed for studied PCMs. It can be seen that most of the research on phase change problems have been carried out within the temperature range 0–65°C suitable for domestic heating/cooling [5].

When it comes to space heating systems, their operating temperature is influenced by several factors, including the heat transfer media, heating terminal devices, heat generation devices, and the thermo-physical properties of the building envelope [7]. The temperature needed on the demand side is dictated by comfort needs, whereas the temperature on the source side is related to the heating source in the system. When fossil fuels are used, the temperature difference between the source and the comfort range is usually very large. However, with solar heating, the choice is limited because a higher phase change temperature results in a higher temperature at the collector outlet, which can negatively impact the efficiency of the solar collector. [16]. Looking at Table 2.1 it can be seen that the PCM selection is extremely case-sensitive. The combination between heat pumps (HPs) and LHTES systems is rather flexible thanks to the abundant variety of refrigerant fluids accessible for heat pumps [7]. For this reason these two technologies can be adopted in a wide range of operational temperatures. Different is the situation for LHTES in residential solar systems, where typically the operative temperature is placed in the restricted medium-to-low temperature range (45 – 55°C). When looking instead at the adoption of LHTES units in combination with micro-CHP or district heating (DH) systems the operative temperature shifts to higher values (>65°C) [7].

Table 2.1: Different PCMs characteristics and applications (adopted from [7, 31])

PCM	T_{pc} [°C]	Δh_{pc} [kJ/kg]	Application	Ref.
Inorganic	29	191	HP	[32]
Organic	40	220	HP	[33]
Inorganic	46	210	HP	[34]
Inorganic	46	210	HP, solar	[35]
Organic	47	142	HP	[36]
Inorganic	48	210	HP	[37]
Inorganic	48	201	HP	[38]
Organic	49	180	HP	[39]
Organic	50	200	HP, solar	[40]
Organic	52	168	solar	[41]
Inorganic	52.4	220	solar	[42]
Inorganic	53	224	HP	[43]
Organic	54	200	HP, solar	[44]
Inorganic	58	266	HP	[45]
Organic	58	172	HP	[46]
Inorganic	58	266	HP	[43]
Organic	61	222	HP	[43]
Organic	64.5	208	micro-CHP	[47]
Organic	70	260	DH	[48]

2.3 PCM containers for LHTES

Once the PCM has been selected, based primarily on the temperature range of application, the next step consists in choosing the geometry of the PCM container as well as the thermal parameters of the container required for a given amount of PCM. Each of these factors directly influence the heat transfer characteristics in the PCM and ultimately affects the melt time and the performance of the PCM storage unit.

A storage system using a heat exchanger is comprised of a storage vessel that contains the storage medium (the PCM) and an internal heat exchanger.

The heat transfer fluid (HTF), e.g. water, flows through the heat exchanger and exchanges heat with the phase change material in the storage vessel. The heat exchanger generally consists of multiple pipes homogeneously distributed throughout the storage volume in a shell-and-tube configuration [7]. PCMs are usually placed in long thin heat pipes, cylindrical or rectangular containers [5]. Looking at Figure 2.3, the schematics of the cylindrical and rectangular containers are given. The most analysed LHTES unit is the shell-and-tube system, indeed more than 70% of TES use them [5]. This is likely because most engineering systems use cylindrical pipes, and also because heat loss from the shell-and-tube system is very little.

Going back to the different cylindrical PCM container configurations, three main possibilities are available [5]. The first one is where the PCM fills the shell while the HTF flows through a single tube (Figure 2.3a). In the second possibility, instead, the PCM fills the tube while the HTF flows parallel to the tube (Figure 2.3b). The last one is the shell-and-tube system (Figure 2.3c), usually adopted to improve heat transfer in PCMs [5]. Agyenim et al. [49] developed an experimental energy storage system to compare horizontal shell-and-tube heat exchanger with 4 tubes and a pipe model using a medium temperature PCM (erythritol) whose melting point is equal to 117.7°C. Heat transfer in the shell and tube system was primarily influenced by the effect of multiple convective heat transfer rather than conductive heat transfer in the pipe model. The initiation of natural convection, which forms multiple convective cells in the shell-and-tube system, notably changed the fluid flow pattern at the solid-liquid interface, resulting in complete melting within 5 hours, compared to over 8 hours for the pipe model. For these reasons the authors [49] suggested the shell-and-tube configuration for the charging of the PCM.

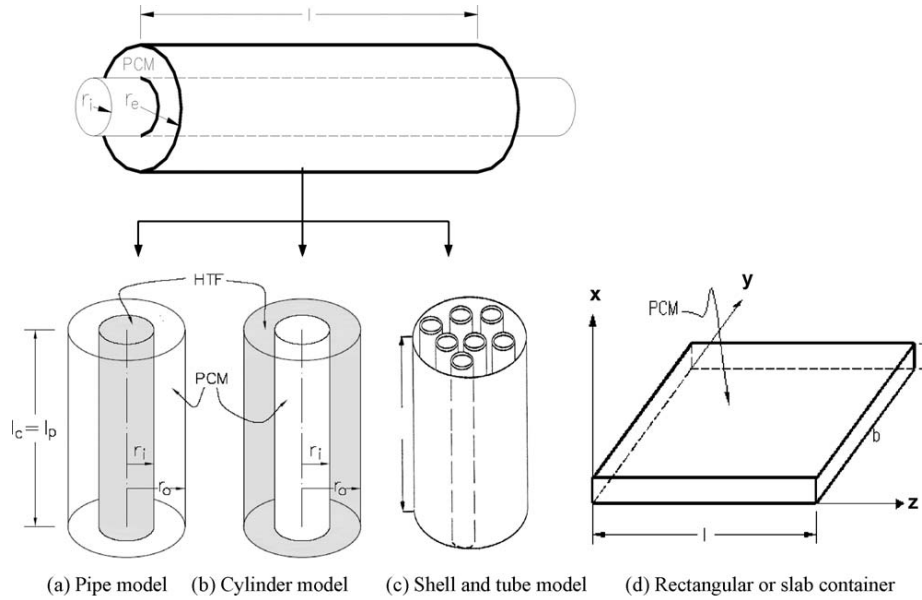


Figure 2.3: Configuration classification of commonly used PCM containers [5]

2.4 LHTES fins design approaches

As evidenced in the previous section, the shell-and-tube configuration for the LHTES is the most studied. This is because of the many advantages that this solution provides, such as the simple design, relatively cheaper and very smaller pressure drop than other solutions, large heat transfer area, high discharging power, and overall high effectiveness [50]. For these reasons the shell-and-tube heat exchanger type of LHTES is the most widely employed solution. Hence this thesis is focused on the modelling of a few shell-and-tube LHTES units. An overview on the design approaches suitable for the shell-and-tube LHTES is here provided.

As already discussed, one of the major problems concerning PCMs in LHTES is their low thermal conductivity. As a consequence, the energy that can be exchanged between the HTF flowing in the pipes and the PCM stored in the heat exchanger is limited for a given period of useful time. As mentioned in Section 2.2, one of the solutions available to address this problematic is the use of high conducting fins, which are necessary to reduce

the average diffusion distance between the HTF and the PCM [7]. Of course, the optimization of the fins' geometry has been a matter of great importance in the field of LHTES for several years. Numerous studies are available in the literature, which discuss many topics of interest, starting from the material preparation methods to the thermo-physical properties.

From the most recent reviews [51, 52, 53, 54, 55], the following five fin layouts are the most studied:

- Longitudinal;
- Circular;
- Helical;
- Y shaped;
- Pins.

Between the aforementioned layouts, the longitudinal one is the most used extended surface geometry in LHTES, reaching 60% of installations [51]. This development is probably due to an easy design and fabrication and high efficiency in the heat-transfer [56]. Longitudinal fins usually have a rectangular shape and are located along the axis of the inner tube to extend the heat-transfer surface between the PCM and the HTF. Research by Solomon [57] showed the effect of the fin height on the solidification performance of the PCM. The longitudinal fin proves most effective when the surface heat flux is high. With a height of approximately 60% of the annular gap size, it achieves maximum enhancement in heat transfer for the analyzed configuration. However, a conflicting effect was observed during the sensible cooling of the liquid PCM. This is attributed to a reduction in free convection within the liquid PCM due to the presence of the fin [57]. Study by Yuan et al. [58] identified an optimal tilt angle of longitudinal fins that enhances convective transport in LHTES unit in horizontal configuration. Al-Abidi et al. [59] designed internal and external fins for a triplex tube heat exchanger to enhance the phase change rate of the PCM, using both numerical and experimental works. They analysed different operation parameters, such as the fin length, fin thickness, number of fins, Stefan number and PCM unit geometry. The results highlighted that the fin length and the number of fins strongly affect the melting rate whereas the fin thickness is not relevant [59]. Rathod and

Banerjee [60] evaluated the thermal enhancement in shell-and-tube LHTES with longitudinal fins, resulting in a 24.5% reduction in melting time and a 43.6% reduction in solidification time.

Circular fins are not studied as much as longitudinal ones when considering LHTES systems. However, thanks to their straightforward design and ease of production, the development of this concept is not negligible, as evidenced by the large number of recent studies [52, 61]. In a shell-and-tube TES device, a circular fin refers to a radially extending heat transfer surface that is attached to the tube's wall. Mosaffa et al. [62] developed an analytical model to predict the PCM solidification process in a circular finned shell-and-tube TES. During the melting process, the liquid fraction is proportional to $Fo \cdot St^{3/4}$ (Fourier and Stefan numbers), whereas the Nusselt number is proportional to $St^{1/4}$ [63]. In order to fully utilize natural convection during the melting process, numerous novel circular fin configurations have been suggested in the literature. The natural convection heat transfer is significant during the melting of PCM, especially in the upper portion of a vertical TES. Gravity exerts a force that enhances natural convection in the upper region of the thermal energy storage system, while the lower part remains dominated by conduction. Singh et al. [64] studied the the best-finned configuration at constant fin volume fraction. Three different finned cases using equal height, increasing as well as decreasing height of fins were investigated as shown in Figure 2.4. Because of the optimum use of natural convection in the decreasing finned TES arrangement, a reduction equal to 43% for the total melting time is achieved [64].

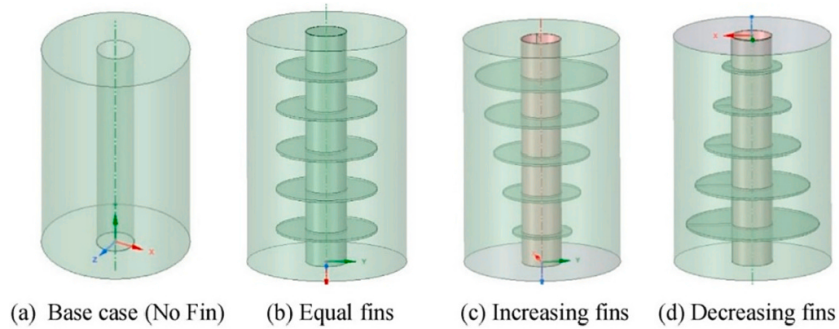


Figure 2.4: Schematic diagram of uniform and non-uniform fin height [64]

The designers should optimize the fin geometry and pitch to balance improved heat diffusion with the reduced buoyancy effect, thereby maximizing the overall enhancement. Some researchers attempted to design perforated fins to improve heat transfer and facilitate the flow of liquefied PCM. Karami and Kamkari [53] experimentally compared the heat transfer enhancement of solid and perforated fins in a LHTES. The results showed that fins with small holes achieved Nusselt numbers approximately 30% higher than those of the solid fin configuration, while also reducing the melting time by 7%. Circular fin parameters such as fin height, pitch, number, angle and material have also been studied. Kalapal and Devanuri [65] experimentally and numerically evaluated the effect of orientation on the melting behavior of the PCM in a LHTES adopting circular fins. The results evidenced that the vertical orientation led to the fastest melting rate. Then, it can be concluded that the trade-off between the enhancement of the thermal conductivity and the natural convection is the key problem. Thus, the identification of an optimum design rule for circular fin is crucial. Another important aspect of circular fins concerns the fin thickness, which is typically 1–2 mm. As a consequence, the volume expansion of the phase change material may cause significant stress on circular fins after numerous cycles [56].

The helical fin design approach has been implemented in LHTES only recently. Rozenfeld et al. [66] designed a shell-and-tube LHTES unit with helical fins attached to the inner tube. The experimental results demonstrated that, compared to traditional fins, the helical fin accelerated the melting rate, reduced the pressure during the melting process, and prevented void formation during solidification. Furthermore, based on the experimental data, they determined an analytical model including the Fourier, Stefan, Archimedes, Prandtl numbers and a dimensionless geometrical parameter in order to give a complete generalization of the results [66]. Zhang et al. [67] analysed the melting performance of paraffin wax in LHTES using different fin configurations, including various helical fin designs. The results showed that the flow rate of liquefied PCM in the helical fin configuration is lower than in the longitudinal configuration, but the vorticities in the helical fin setup are larger and stronger. Consequently, the melting rate in the helical fin configuration is significantly higher. This result highlights the crucial role of vorticities in the melting process, as they enhance natural convection [67]. Caron-Soupart et al. [68] analysed the heat transfer performance of different LHTES units. Experiments showed that the copper tube with helical fins

system is the first to complete the charging process followed by the steel tube with longitudinal fins system. The researchers also stated that the charging process is dominated by natural convection. After what has been stated, it can be concluded that the heat transfer performance of helical finned TES is better than that of traditional finned TES. In the helical fins solution, both natural convection and the formation of vorticities present remarkable effects on the melting process of the PCM [56].

The design of Y-shaped fins (also known as tree fins) was created to increase the performance of classical longitudinal fins. Sciacovelli et al. [54] evaluated the thermal behaviour of the system using a CFD model and the response surface method in order to optimize the fin length and bifurcation angle. An increase of 24% of the system efficiency can be achieved by the optimized system using the developed fin design. In a following article [69], the authors found an optimized tilt angle along the longitudinal direction such that the solidification time is reduced (i.e. the discharge process of the system). The analysis of entropy generation in the storage system was used to drive the design process and to identify the most relevant changes in the design of the fins. Lately, less conventional shapes are explored by researchers, like the snowflake-shaped fin geometry (see Figure 2.6a) outlined by Sheikholeslami et al. [70]. The fin geometry was optimized by the response surface method. Results showed notable performance enhancements over traditional longitudinal fins, resulting in a solidification rate 2 times faster [70].

A cooling technique for electronic applications in TES systems, is considered one of the methods that have been extensively studied over recent years [7]. However, a critical challenge in the design of the PCM based on electronic cooling systems is the undesirable property of PCMs: low thermal conductivity. To overcome this drawback, PCMs based on heat sinks with pin fins were widely utilized for the cooling enhancement of electronic products. The heat enhancement factor was effectively dependent on increasing the numbers and dimensions of these fins. In the review [55] on heat transfer enhancement in LHTES, this layout is only listed as a suitable alternative to plate fins for maximum heat dissipation in heat sinks. When considering pin fins in LHTES, natural convection must be taken into account since pins permit almost unrestricted movement of buoyant eddies [71].

The fins that were discussed in this section had all in common the pre-

defined shape restriction. This limit can hamper the achievable performance of the LHTES system. A solution to this problem resides into topology optimization, which enables the most efficient distribution of material to enhance the thermal performance [7]. The great advantage of such approach is given by the design freedom, thus no assumptions are needed when using this design strategy. Let's consider shape optimization. Such method involves the imaginary drilling of "holes" in an high conductive material (HCM) block to determine the optimal shape [7]. The limit of such optimization method concerns the fixed number of holes which have to be determined a-priori. In the work done by Pizzolato et al. [72], the topology optimization problem was formulated using a density-based method. The results obtained in the article demonstrate the convenience of topology optimization for the practical design of LHTES systems. The method yields design features and trends that could hardly be revealed with alternative design routes.

To conclude the section on fins, it is important to note that when implementing a shell-and-tube LHTES unit, various practical considerations must be taken into account. In particular, the optimal fins design may need to be adjusted to accommodate real-world limitations and balance cost with performance [7]. For further investigation on the topic, the reader is suggested to check [7].

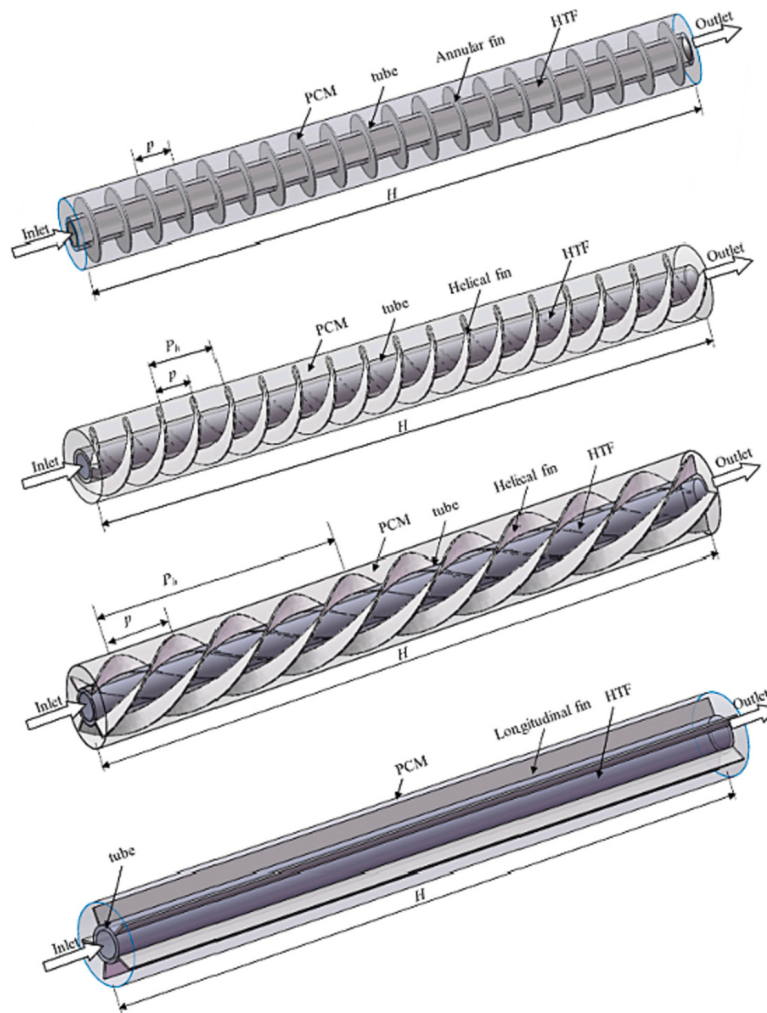


Figure 2.5: Comparison of a circular fin, helical fin and longitudinal fin LHTES unit [56, 67]

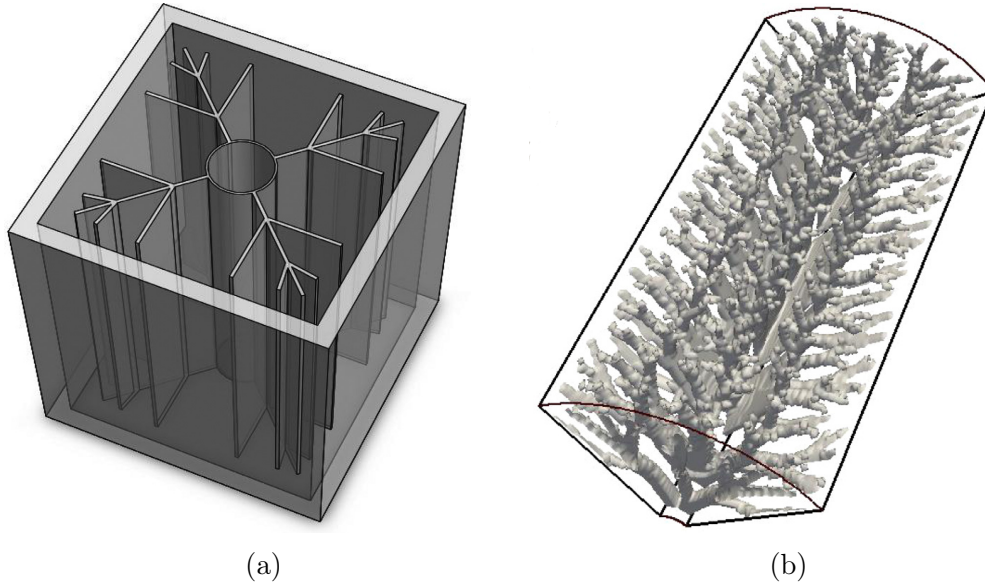


Figure 2.6: (a) Three dimensional view of Snowflake shaped fin [70], (b) 3D design visualization of a sectioned finned unit using topology optimization [72]

2.5 State of the art on LHTES modelling

The phase change process involves a dynamic boundary (∂D_{ls}) that distinguishes the liquid domain (D_l) from the solid domain (D_s) [7]. A simplified graphical representation of the process is depicted in Figure 2.7.

The process is quite complicated to model if no simplifying assumptions are made. Hence the following hypotheses are set: negligible advective transport, constant density, constant specific heat and precise melting temperature. If these assumptions are considered, then the following equations can be used to describe the change of phase process [7]:

$$\rho_s c_{p,s} \frac{\partial T}{\partial t} = \nabla \cdot (k_s \nabla T) \quad \text{in } D_s \quad (2.3)$$

$$\rho_l c_{p,l} \frac{\partial T}{\partial t} = \nabla \cdot (k_l \nabla T) \quad \text{in } D_l \quad (2.4)$$

$$T = T_{pc} \quad \text{on } \partial D_{ls} \quad (2.5)$$

$$k_s \nabla T - k_l \nabla T = \rho_s \Delta h_{pc} u_{\partial D_{ls}} \quad \text{on } \partial D_{ls} \quad (2.6)$$

where ρ_s and ρ_l are the solid and liquid densities respectively, $c_{p,s}$ and $c_{p,l}$ are the solid and liquid specific heat capacities, k_s and k_l are the conductivity tensors of the solid and of the liquid phases, Δh_{pc} is the latent heat capacity, $u_{\partial D_{ls}}$ is the normal propagation velocity of the solid-liquid interface and T_{pc} is the average phase change temperature. Eq. 2.3 and Eq. 2.4 describe the heat diffusion in the solid and liquid domains respectively. Eq. 2.5 identifies the phase change front. Eq. 2.6 is known as the Stefan condition [7, 73] and it represents the heat balance at the moving front.

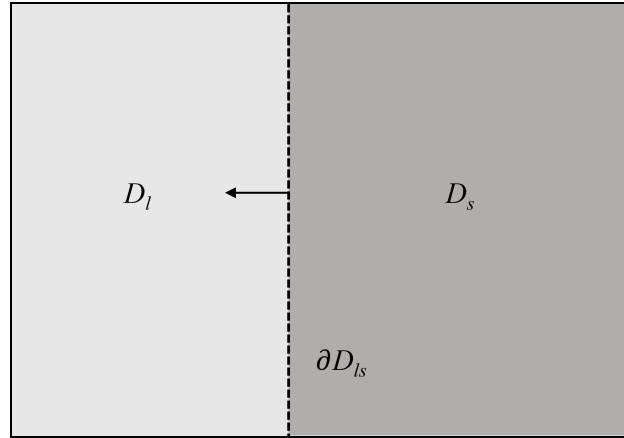


Figure 2.7: Solid-liquid interface during the PCM phase change process [7]

When considering the phase change problem, the simplest one is the one-phase problem first solved analytically by Stefan [74, 75]. It is important to notice the "one phase" term, which means that only one of the phases (liquid) is active, whereas the other phase stays at its melting temperature. Stefan's analysis, which assumes constant thermo-physical properties, indicates that the rate of melting or solidification within a semi-infinite area is dictated by a dimensionless parameter, called the Stefan number (St) ($St = c_p \Delta T_{pc} / \Delta h_{pc}$). Neumann [74, 76] extended the Stefan's solution to the two-phase problem (Neumann's method). Now, the initial state of the PCM is assumed to be solid, for a melting process, but its initial temperature is not the same as

the phase change temperature, and its temperature during the melting is not kept at a constant value.

Numerical methods for solving the pure heat conduction equation with a phase change involved can be classified as either fixed grid methods or variable grid methods [74]. In the fixed grid methods, the heat flow equation is approximated by finite difference replacements for the derivatives in order to compute values of temperature $T_{i,n}$, at $x_i = i\Delta x$ and time $t_n = n\Delta t$ on a fixed grid in the (x, t) plane [74]. As the name of the method suggests, the numerical solution is carried out on a space grid that remains fixed throughout the calculation. The primary benefit of these methods is their ability to efficiently manage multidimensional problems with ease. Consequently, the numerical treatment of the moving boundary can be accomplished through straightforward modifications to existing heat transfer codes [74]. The stability of fixed grid methods can be jeopardized if the boundary moves more than a single space increment within one time step. This limitation, associated with the velocity of the moving boundary, can significantly increase both memory usage (due to larger array sizes) and CPU time during extended computations [74]. The problems associated with the fixed grid method can be avoided by using the variable grid methods. According to these methods, the exact location of the moving boundary is evaluated on a grid at each step. The grid can be either interface fitting or dynamic.

The methods described above are termed strong numerical solutions because they emphasize using finite difference techniques on the strong formulation of the process, identifying moving boundaries, and determining temperature profiles at each time step [74]. These are applicable to the problems involving up to two phases in one space dimension. For two-dimensional cases they are no more applicable and more complicated approaches are requested [74]. Another approach is to utilize what are known as weak numerical solutions. These methods reformulate the problem so that the Stefan condition is implicitly integrated into a new set of equations, which apply across the entire fixed domain. This approach avoids focusing specifically on the nature of the moving boundary [74]. Many methods of latent heat evolution exist, but only a small selection is going to be discussed in the following, and these are:

- Apparent heat capacity method;

- Effective capacity method;
- Source based method;
- Enthalpy method.

2.5.1 Apparent heat capacity method

In this method, the latent heat is considered by increasing the heat capacity of the material in the phase change temperature range. If in the phase change temperature range the latent heat is released uniformly, then the apparent heat capacity can be defined as [74]:

$$c_{app} = \begin{cases} c_s, & T < T_s & \text{solid phase} \\ c_{in}, & T_s < T < T_l & \text{solid/liquid phase} \\ c_l, & T > T_l & \text{liquid phase} \end{cases}$$

where:

$$c_{in} = \frac{\int_{T_s}^{T_l} c_p(T) dT + \Delta h_{pc}}{(T_l - T_s)} \quad (2.7)$$

The energy equation then becomes:

$$\rho c_{app} \frac{\partial T}{\partial t} = \nabla \cdot (k \nabla T) \quad (2.8)$$

Eq. 2.8 can easily be discretized and solved numerically.

The apparent heat capacity method was first introduced by Hashemi and Sliepcevich [77] using a finite difference formulation based on the Crank–Nicolson scheme. This method is quite simple, but it is important to state that it does not perform well when for example, considering a melting case, if the temperature of a control volume increases from below the solidus to above the liquidus temperature within a single time step, the absorption of latent heat for that control volume is overlooked (a similar reasoning can be applied for the solidification case) [77]. As a consequence, in this method, in order to overcome said limitation, very small time steps have to be used. It follows then that this method has poor computational efficiency in such scenarios [74].

2.5.2 Effective capacity method

This method was originally developed by Poirier and Salcudean [78] as a way to improve the apparent capacity method. In this model, a temperature profile is assumed between the nodes; instead of assessing an apparent capacity using nodal temperature, an effective capacity is computed by integrating across the control volume. To obtain the effective capacity over the control volume, the following integration is needed [74]:

$$c_{eff} = \frac{\int c_{app} dV}{V} \quad (2.9)$$

where c_{eff} , c_{app} and V are the effective heat capacity, the apparent heat capacity and the control volume respectively.

Despite its accuracy, the effective capacity method is very challenging to implement. The numerical integration is particularly costly, especially when thermal gradients are steep within the phase change temperature range [74].

2.5.3 Source based method

Any additional heat from either a heat source (like the latent heat during the solidification) or a heat sink (like the latent heat during the melting) is allowed to be introduced into the general form of the energy equation as an extra term, i.e. the source term, when considering this method [74]. When the convective transport is negligible, the energy equation can be simplified to Eq. 2.10 [74]:

$$\rho \frac{\partial(c_p T + \Delta h_{pc})}{\partial t} = \nabla \cdot (k \nabla T) + S \quad (2.10)$$

where the source term S is given by the following equation:

$$S = -\rho \frac{\partial \Delta h_{pc}}{\partial t} \quad (2.11)$$

The source-based method has gained considerable popularity over the years due to its relatively high accuracy, particularly for non-isothermal phase change problems, as the latent heat content is directly linked to the temperature of the grid point. Additionally, this method is computationally efficient [74].

2.5.4 Enthalpy method

The enthalpy method is based on the enthalpy formulation, detailed by Voller and Shadabi [79]. For this method, the following equation is used:

$$\frac{\partial H}{\partial t} = \nabla \cdot (k \nabla T) \quad (2.12)$$

where H is the total enthalpy, that corresponds to the sum of the sensible heat and latent heat:

$$H = \int_{T_{pc}}^T \rho c_p dT + \rho f_l \Delta h_{pc} \quad (2.13)$$

where f_l is the liquid fraction. It allows the computation of the change in enthalpy from the energy in the material during the phase change [80]. The general form of f_l can be written as:

$$f_l = \begin{cases} 0, & T < T_s & \text{solid phase} \\ \frac{T-T_s}{T_l-T_s}, & T_s < T < T_l & \text{solid/liquid phase} \\ 1, & T > T_l & \text{liquid phase} \end{cases}$$

Replacing the liquid fraction definition into Eq. 2.13, the enthalpy of the PCM corresponds to:

$$H = \begin{cases} \int_{T_s}^T \rho c_{p,s} dT, & T < T_s & \text{solid phase} \\ \rho \frac{T-T_s}{T_l-T_s}, & T_s < T < T_l & \text{solid/liquid phase} \\ \int_{T_l}^T \rho c_{p,l} dT + \rho \Delta h_{pc}, & T > T_l & \text{liquid phase} \end{cases}$$

With a properly defined temperature-enthalpy relationship, it is possible to model the complete impact of phase change without requiring precise tracking of the phase change front's exact position. This characteristic simplifies numerical solutions, as the continuously shifting phase change region does not need to be monitored across the discrete numerical grid. [79]. In problems where the position of the phase change region is required, however, this may lead to problems, but it can be computed anyways as a post-processing step. Moreover, the obtained solution is independent of the time step and phase change temperature range [74].

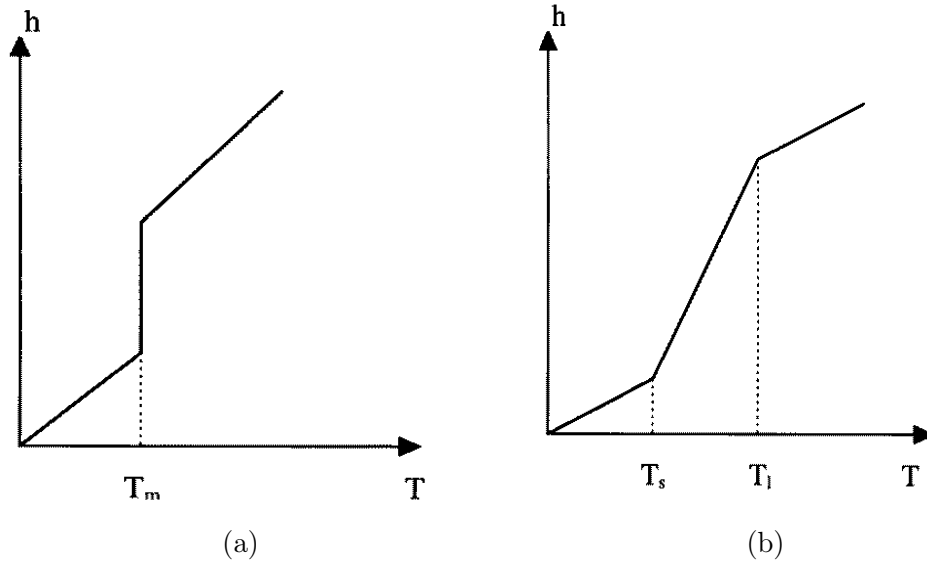


Figure 2.8: Enthalpy as a function of temperature for (a) isothermal phase change; (b) nonisothermal phase change [74]

2.6 LHTES system integration

Integrating LHTES units into building heating systems has been increasingly investigated as a heat load management technology in the last years. However, as is reported in [6], the suggested TRL of multiple lab based LHTES lies in the 5 to 7 range, while only a small number of commercial solutions have demonstrated their effectiveness in real-world operational settings. EASE-EERA [81] states that LHTES which use salt hydrate and paraffin wax are partly commercialised (TRL 6-8). Also, high-temperature (HT) LHTES with integrated finned-tube heat exchangers has been constructed and operated with variable phase-change temperatures between 140°C and 305°C . These HT storages have reached a TRL of 7. This low levels can be ascribed to the economical aspects related to PCMs [81]. Indeed, materials for use as PCMs are still expensive and not always reliable.

The conventional method of integrating LHTES with heat pump-based heating systems involves connecting the heat pump's condenser to charge the LHTES unit. However, this integrated setup typically results in higher electricity consumption for the heating system. Xu et al. [82] presented three

new LHTES integrating layouts in order to try to solve this issue. A LHTES tank with cylindrical PCM encapsulation was modelled as the heat storage device in the heating system. The results obtained by the simulation show a 22 - 26% higher weekly performance factor than the conventional integration layout where the main condenser is utilized for charging. Another advantage obtained by the proposed new layouts is given by the reduction in CO_2 emissions, which can be reduced up to 14% because of less carbon intense electricity production during the on-peak hours [82].

Laing et al. [83] developed a design for heat transfer enhancement using radially finned tubes and it was applied in a 700kWh PCM storage demonstration module. This was integrated into a 1MW pilot direct steam generation power plant in Spain. The PCM storage module effectively operated under both constant and sliding pressure modes to evaporate water. They conducted tests on this component using three distinct operational modes for discharging the PCM storage, all of which were successful. This testing highlights the potential for future cost reductions across the entire storage system. Furthermore, it suggests the possibility of removing either just the recirculation pump or even the entire circulation cycle, including the steam drum [83].

Guelpa and Verda [84] presented a review for the implementation of TES in district heating (DH) and district cooling (DC). The potential of different TES units in combination with DH are analysed, including LHTES solutions. Unfortunately, only a few examples of application of LHTES to DH systems are available. For example, the use of paraffin waxes is being explored as PCM for thermal peak shaving in [85]. Another example is given by the absorption chiller and PCM storage in DC system analysed in [86].

It is hence clear that the application of LHTES in space heating is only limited to few examples, and this can be mainly blamed to the still expensive cost of PCMs and the fact that they are not always reliable [81]. Substantial progress is required before the laboratory-validated PCM molecules can be scaled up for extensive adoption and their long-term stability improved.

Chapter 3

Three-dimensional LHTES models

This chapter main objective is the description of the different three-dimensional LHTES models used to simulate the discharging behaviour of their respective shell-and-tube LHTES units. Different fins geometries and PCM materials are analysed.

Section 3.1 provides an overview on the main COMSOL Multiphysics characteristics.

Section 3.2 focuses on the description of the PCM and fins design choices.

Section 3.3 gives a detailed description of the numerical model adopted to simulate the LHTES heat exchanger discharging behaviour.

3.1 Brief overview on COMSOL Multiphysics

The three-dimensional models are developed using the software COMSOL Multiphysics 6.1. COMSOL Multiphysics is a simulation platform that provides fully coupled multi-physics and single-physics modelling capabilities. It integrates various physics-based modules that allow users to create models in fields such as electromagnetics, structural mechanics, chemical reactions, fluid dynamics and heat transfer. The last two are the ones of interest for this thesis. The "Model Builder" includes all of the steps in the modelling workflow, from defining geometries, material properties, and the physics that

describe specific phenomena to performing computations and evaluating the results. COMSOL Multiphysics employs finite element analysis (FEA) for solving partial differential equations (PDEs) that describe physical phenomena. The software supports various types of meshing and provides tools for refining the mesh to improve accuracy. When the model is developed, it is possible to use the Application Builder to turn it into a simulation application with a dedicated user interface.

3.2 Geometry and materials

3.2.1 PCM design

When designing a LHTES heat exchanger, an important option that has to be carefully analysed is the choice for the material used for the phase change material. As already mentioned in Section 2.2.2, multiple choices are available, each one with its own advantages and disadvantages. In this thesis the materials that are going to be analysed are a paraffin and a salt hydrate, whose properties can be seen in Table 3.1 and Table 3.2. The choice for these two types of material lies in the fact that they have a medium melting temperature (60 - 80°C) and are the materials used in LHTES heat exchangers with the highest Technology Readiness Level. Indeed, the first driving parameter is the PCM melting temperature and it needs to be compatible with the operating temperature range. Another important requirement for the PCM choice lies in the PCM energy density. Higher values are preferred to reduce the overall occupied volume and increase their competitiveness with traditional sensible storage units [7].

Regarding the first material, this is a bio-based paraffin. It has an average melting temperature equal to 71°C and a melting/solidification temperature range of 3°C. Thanks to its organic nature, it is not toxic nor flammable in its operative range. Furthermore, it has an excellent chemical compatibility with the most common high conductive materials used for shell-and-tube fins and pipes [7]. The second material that has been chosen is a salt hydrate with an average melting temperature equal to 72°C and a melting/solidification temperature range of 3°C. In the following tables are listed the materials' properties:

Table 3.1: Paraffin thermal and physical properties (adopted from [7])

Property	Units	Value
Average melting temperature	°C	71
Latent heat of melting/crystallisation	kJ/kg	224
Density	kg/m ³	858
Thermal conductivity	W/mK	0.28
Flash point	°C	288
Specific heat capacity	kJ/kg°C	1.8
Thermal cycles without change in properties	-	10000

Table 3.2: Salt hydrate thermal and physical properties

Property	Units	Value
Average melting temperature	°C	72
Latent heat of melting/crystallisation	kJ/kg	155
Density	kg/m ³	1666
Thermal conductivity	W/mK	0.58
Specific heat capacity	kJ/kg°C	2.13
Maximum operating temperature	°C	120

Finally, no volume or mass constraint are imposed, but a compact solution is more attractive if compared to sensible storage units. Hence the same volume is set for both materials. To find the needed volume, if we consider a typical residential condominium with 8-10 users (roughly 2500m³) in Turin, the availability of a 40kWh thermal energy storage would remarkably reduce the morning peak demand on the district heating network (depending on the season) [7]. The stored energy content can be computed through the following equation:

$$E_{stored} = M_{PCM}\Delta h_{lat} + M_{PCM}c_{p,s}(T_{pc} - T_{min}) + M_{PCM}c_{p,l}(T_{max} - T_{pc}) \quad (3.1)$$

where M_{PCM} is the mass of the PCM stored in the LHTES unit, Δh_{lat} is the average PCM's latent heat content, $c_{p,s}$ and $c_{p,l}$ are the PCM specific heat capacity when solid and liquid respectively, T_{pc} is the average phase change temperature, T_{min} and T_{max} are the design minimum and maximum

temperature of the heating system respectively. From this equation, once we know the needed stored energy, we can find the volume necessary to reach the goal. The PCM total volume is approximately equal to $573.448 \cdot 10^{-3} \text{ m}^3$ for the paraffin to reach the wanted stored energy content. The same volume is kept also for the salt hydrate configuration for simplicity.

3.2.2 Fins design

As already discussed in Section 2.4, when designing a LHTES heat exchanger, many fins design approaches can be followed to increase the thermal conductivity of the PCM-HCM assembly [7]. Overall, we can identify two main criteria that can be followed. The first one is focused on minimizing the overall time needed to store/release a specific amount of thermal energy. The speed of discharge is hence maximized. The second one, instead, is focused on guaranteeing a steady heat transfer rate when the LHTES is discharged [72]. In LHTES units, the heat travels by diffusion from the internal pipes to the PCM [7]. This leads to an exponential decreasing trend in time for the average temperature difference and the thermal power output. Another important factor to consider is the type of process said fins have to be optimized for, i.e. discharging or charging process [87]. This difference arises due to the varying primary heat transfer mechanisms. During the PCM melting process (charging), convective heat transfer becomes significant due to the increase in the liquid fraction of the PCM. Conversely, during the PCM solidification process (discharging), heat diffusion dominates once a solid PCM layer forms around the fins and pipes [7, 88].

The LHTES considered for this study is developed accordingly to the use of the LHTES prototypes realized by [7], hence the main goal is to design the fins such that the discharging process is the fastest possible. Another consideration that has to be taken into account is the popularity in the LHTES heat exchangers adopted solutions for fins. Following all the aforementioned properties and constraints, two types of fins are going to be analysed in this thesis and they are:

- longitudinal fins;
- circular fins.

Following the same manufacturing idea proposed in [7], aluminium matrices fitting the profile of the copper pipes are used to create the different fins distribution. In the longitudinal fins solution the aluminum matrix is made of 12 equally spaced fins (1mm thick) following an hexagonal perimeter. This is done by alternating longer and shorter fins (30mm and 25mm respectively). The fins are extended to their maximum length to reach the farthest areas of the PCM, while simultaneously avoiding contact with the surrounding pipes. Instead, in the circular fins solution the aluminum matrix is made of 125 equally spaced fins (1mm thick, 10mm pitch). The fins have a diameter of 62mm so that the same volume of HCM is kept between the two different fins configurations. In the following tables are listed the different LHTES models geometric and thermo-physical properties. Also, a graphical representation of the computational domains is given in Figure 3.1 and Figure 3.2 for the two different fins configurations. As can be seen, they actually represent a reduced domain thanks to the geometrical and thermal symmetry of the assembly.

Table 3.3: Pipe geometrical characteristics

Property	Units	Value
Number of pipes	-	96
Inner diameter	m	0.0149
Length	m	1.29
Pipe thickness	m	$0.75 \cdot 10^{-3}$
Matrix thickness	m	0.001

Table 3.4: Copper thermo-physical properties

Property	Units	Value
Density	kg/m^3	8978
Specific heat capacity	$\text{J}/(\text{kgK})$	381
Thermal conductivity	$\text{W}/(\text{mK})$	208

Table 3.5: Aluminum thermo-physical properties

Property	Units	Value
Density	kg/m ³	2701
Specific heat capacity	J/(kgK)	871
Thermal conductivity	W/(mK)	152

Table 3.6: Longitudinal fins geometrical characteristics

Property	Units	Value
Number of fins	-	12 (6+6)
Radial length	m	0.025 / 0.030
Axial length	m	1.29
Thickness	m	0.001

Table 3.7: Circular fins geometrical characteristics

Property	Units	Value
Number of fins	-	125
Diameter	m	0.062
Axial length	m	1.29
Thickness	m	0.001

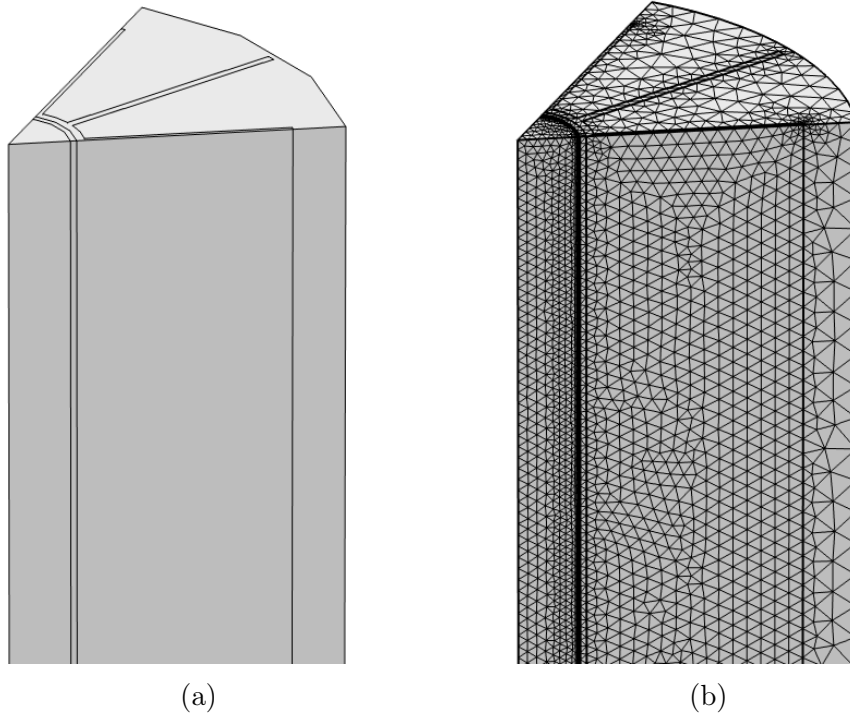


Figure 3.1: (a) Longitudinal fins LHTES domain; (b) Mesh of the longitudinal fins LHTES domain

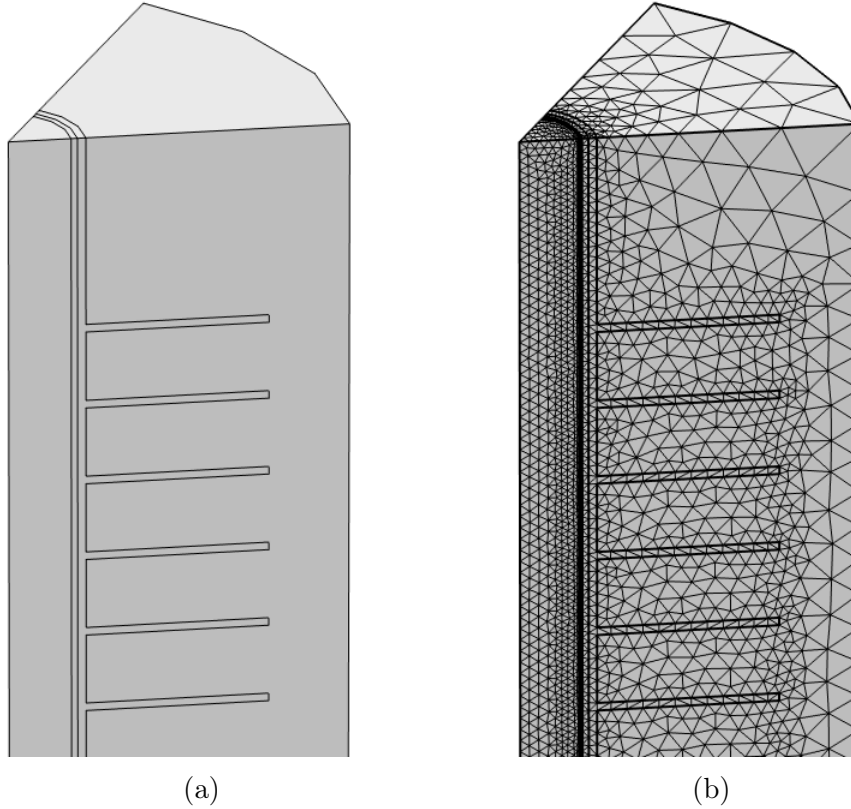


Figure 3.2: (a) Circular fins LHTES domain; (b) Mesh of the circular fins LHTES domain

3.3 Numerical model

3.3.1 PCM's specific heat capacity model

The solidification process of the PCM requires particular attention. Hence, the PCM sub-domain is considered as a solid material whose specific heat capacity c_p is expressed as a function of temperature; a graphical representation of $c_p(T)$ is given in Figure 3.3. With this method, an expression of the specific heat is considered so that the entire latent heat due to condensation is released in the temperature range associated with the phase change (3°C

in this specific case). In the case the specific heat of the solid phase is equal to that of the liquid phase, a Gaussian expression can be adopted for the specific heat:

$$c_p(T) = c_{p,s} + \frac{\Delta h_{lat}}{\Delta T_{sl} \sqrt{\pi}} \exp \left[\frac{-(T - T_{pc})^2}{\Delta T_{sl}^2} \right] \quad (3.2)$$

where $c_{p,s}$ is the the specific heat of the solid PCM, ΔT_{sl} is the condensing/melting temperature range and T_{pc} is the average temperature in the phase change range. Using this expression, the specific heat becomes as represented in Figure 3.3, where the area below the Gaussian function considers also the latent heat.

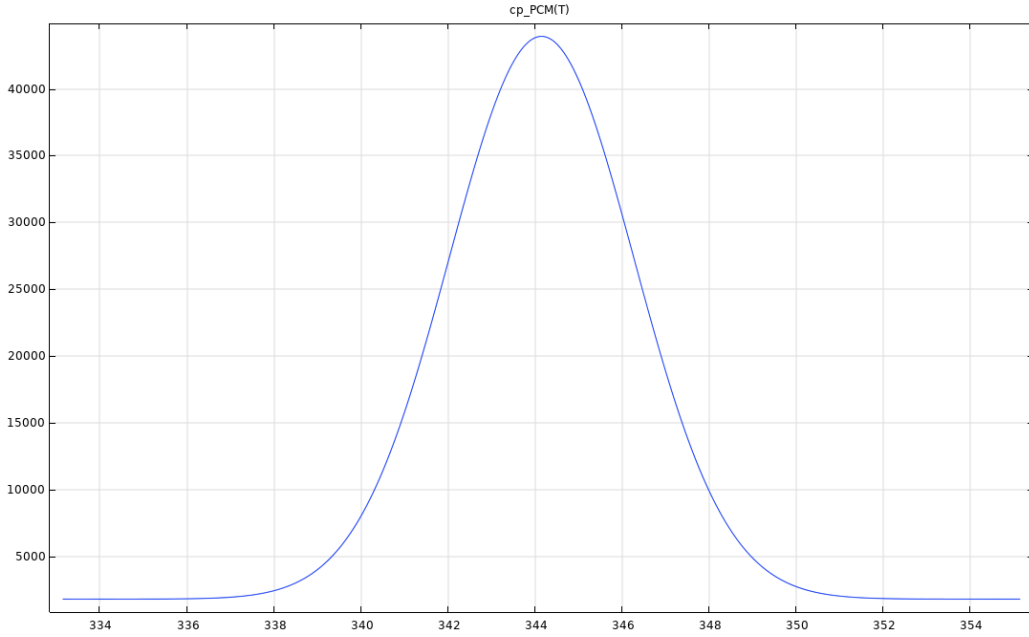


Figure 3.3: Equivalent specific heat for the PCM [J/(kgK)]

3.3.2 Physics, mesh and study

Natural convection phenomenon in the PCM is considered to be negligible with respect to conduction because of the compact design of the LHTES unit [89]. As a consequence, the continuity and momentum equations can only be

applied to the HTF sub-domain (see Eq. 3.3 and Eq. 3.4). The water fluid flow regime is turbulent in the analysed study. The $k-\omega$ turbulence model is hence adopted. When looking at the energy equation instead, the whole computational domain has to be considered, both liquid and solid (Eq. 3.5).

$$\nabla \cdot \mathbf{u} = 0 \quad (3.3)$$

$$\rho \frac{\partial \mathbf{u}}{\partial t} + \rho \mathbf{u} \cdot \nabla \mathbf{u} = -\nabla p + \mu \nabla^2 \mathbf{u} \quad (3.4)$$

$$\rho c_p \frac{\partial T}{\partial t} + \rho c_p \mathbf{u} \cdot \nabla T = \nabla \cdot (k \nabla T) + Q \quad (3.5)$$

The non-isothermal flow multiphysics is set so that it is possible to solve the conservation of energy, mass and momentum in fluids and porous media and for conservation of energy in solids.

Once the equations are set, it is time to define the boundary conditions. Adiabatic walls are considered on bottom, top and external faces of the PCM-HCM assembly; symmetry is imposed on the lateral faces of the PCM-HCM assembly; the entrance of the HTF is a velocity inlet (0.1755m/s) for the turbulent flow study and a fixed temperature (50°C) for the heat transfer study, while the exit is a pressure outlet. As far as the initial conditions are concerned, the initial HTF velocity is null, while the whole domain has a starting temperature of 80°C.

Moving on to the mesh, the computational grid consists of a non-structured polygonal mesh, so that the mesh can conform more closely to complex shapes and boundaries. COMSOL Multiphysics gives the possibility to choose the element size for the mesh from a list of predefined values, which range from "extremely coarse" up to "extremely fine" when the sequence type is for the mesh is "physics-controlled". Otherwise the "user-controlled" option can be selected and a greater customization of the mesh is made available. For the numerical model under analysis, the "extra fine" element size option for the mesh is selected (see Figure 3.1b and Figure 3.2b for a graphical representation). This proved to give the better trade-off between accuracy and computational time.

Once the geometry, the physics and the mesh of the LHTES model are defined, it is possible to start the study of the discharging process. The stationary study is used for the turbulent flow problem to compute the steady

flow and pressure fields. The time dependent study is used instead for the heat transfer problem to compute temperature changes over time. The non-linear method selected is the constant (Newton) where a constant damping factor equal to 0.9 is used in all iterations of Newton's method. The iterative linear system solver GMRES (Generalized Minimum RESidual) with 50 iterations before restart is selected. Convergence is assumed to be reached when the residuals are lower than 10^{-3} . Also, the selected time step is 1s. This value proved to be sufficiently fine not to influence the results.

3.3.3 Post-processing

After the study is performed, the next step is the post-processing. This is a crucial step that involves analysing and visualising simulation results to extract useful information. In COMSOL Multiphysics the "results" section allows to perform such actions. The quantities of interest are computed as surface or volume integrals depending on the studied domain. In the following figures it is possible to see the various plots showing the trend in time for the different LHTES solutions: the PCM average temperature, the average HTF outlet temperature and the average heat flux at the contact wall between the HTF and the PCM-HCM assembly.

- Paraffin, longitudinal fins

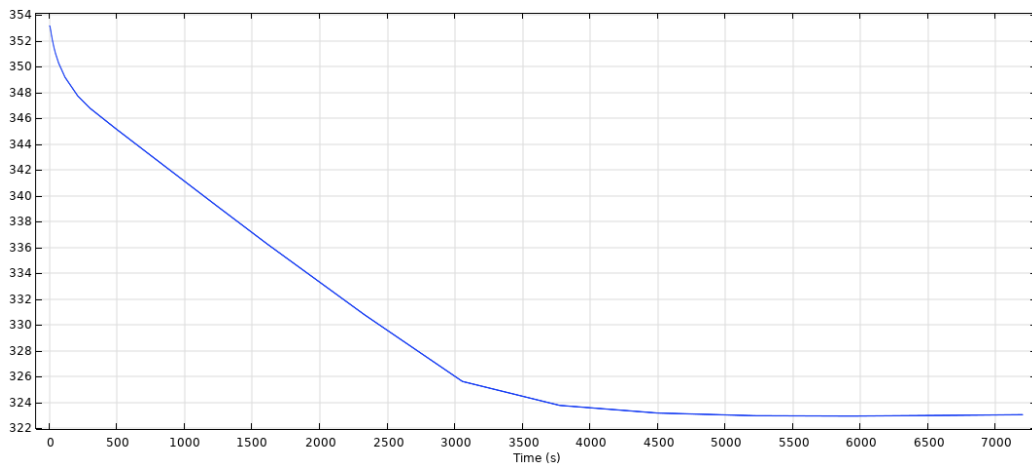


Figure 3.4: Average PCM temperature [K]

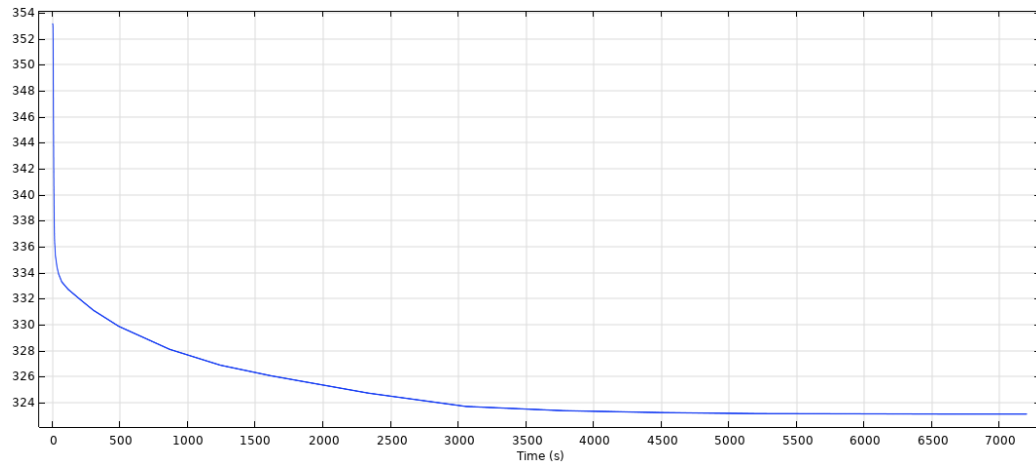


Figure 3.5: Average HTF outlet temperature [K]

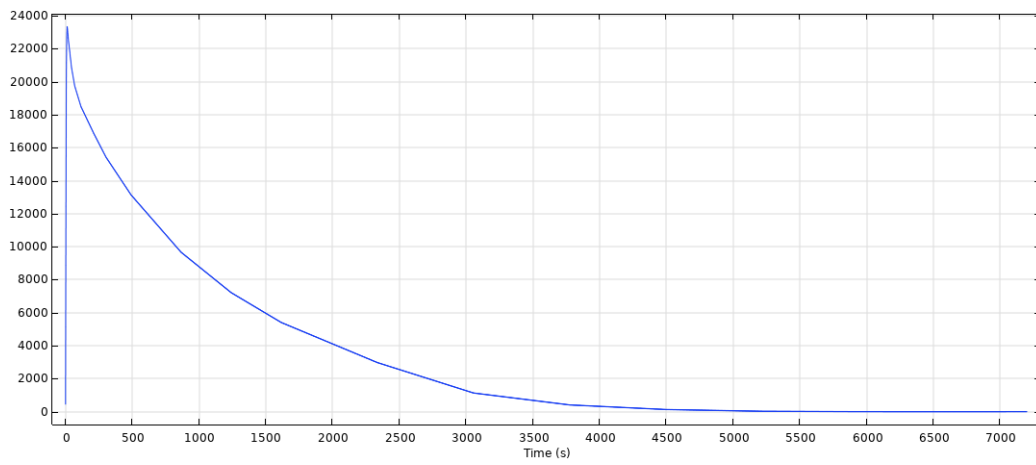


Figure 3.6: Average heat flux [W/m²]

- Paraffin, circular fins

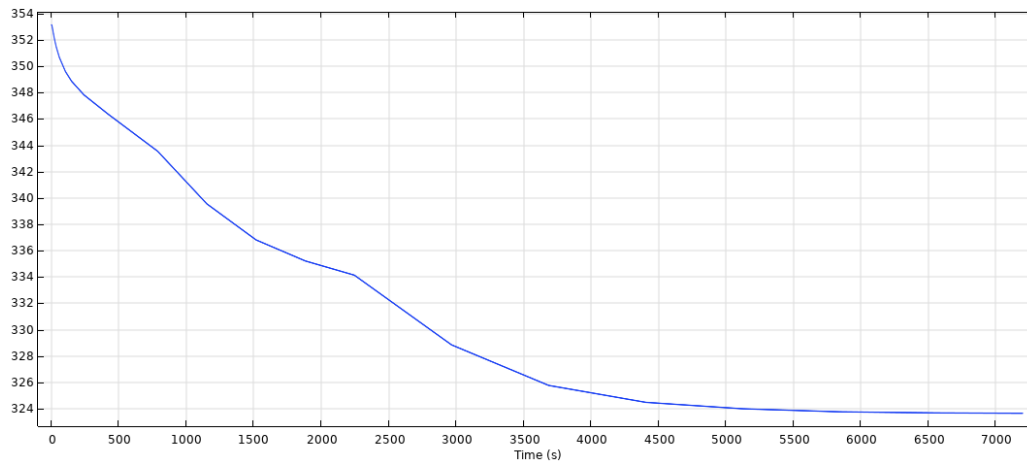


Figure 3.7: Average PCM temperature [K]

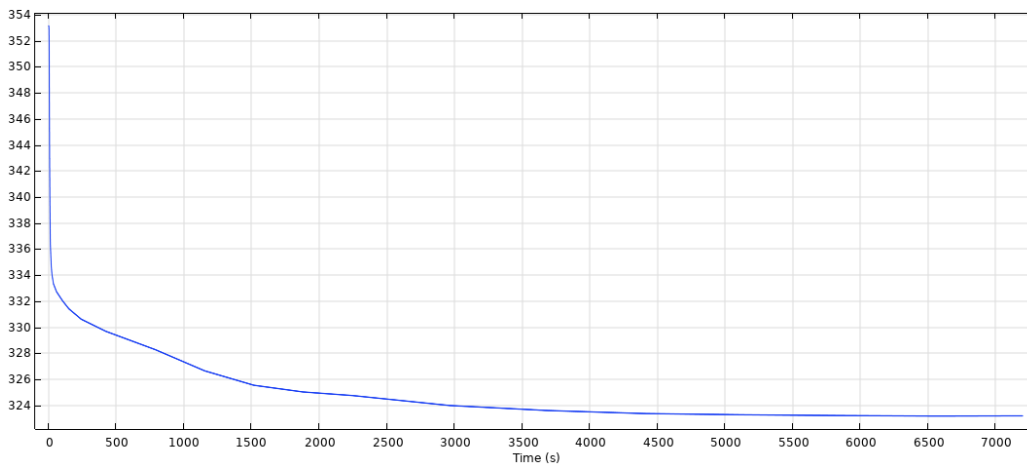


Figure 3.8: Average HTF outlet temperature [K]

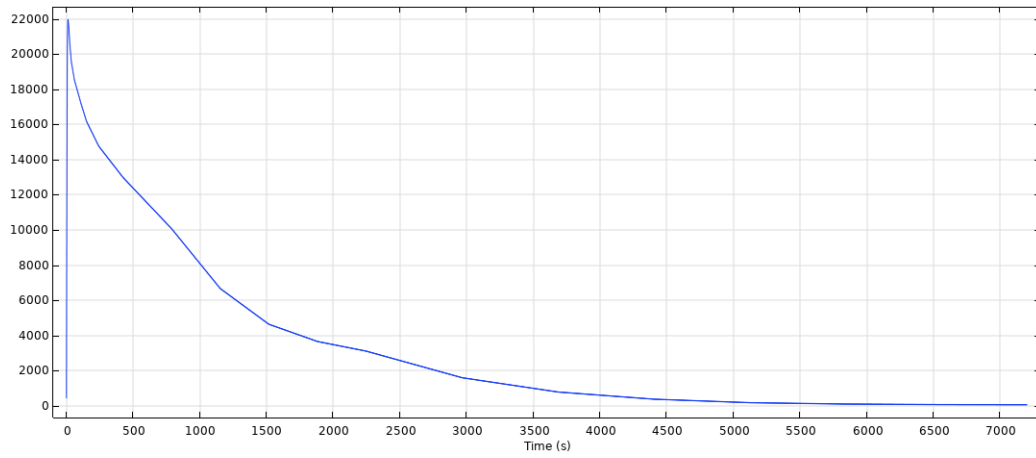


Figure 3.9: Average heat flux [W/m²]

- Salt hydrate, longitudinal fins:

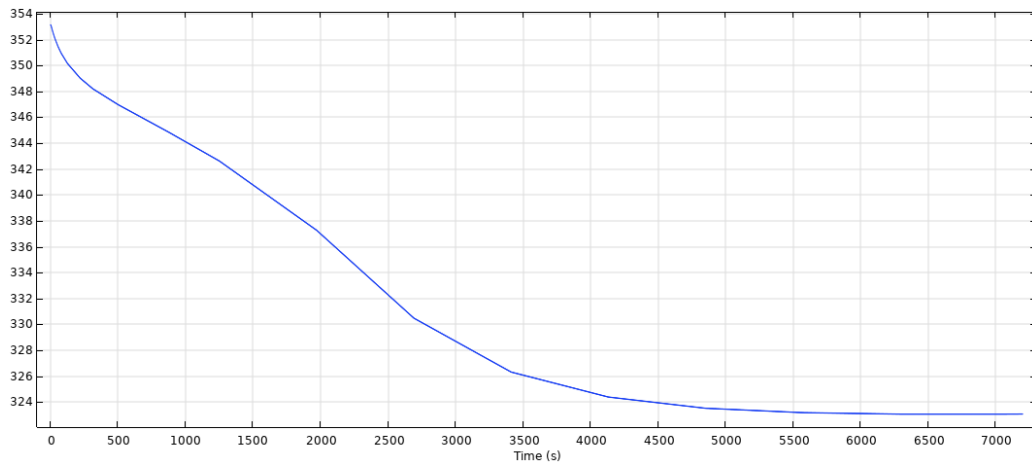


Figure 3.10: Average PCM temperature [K]

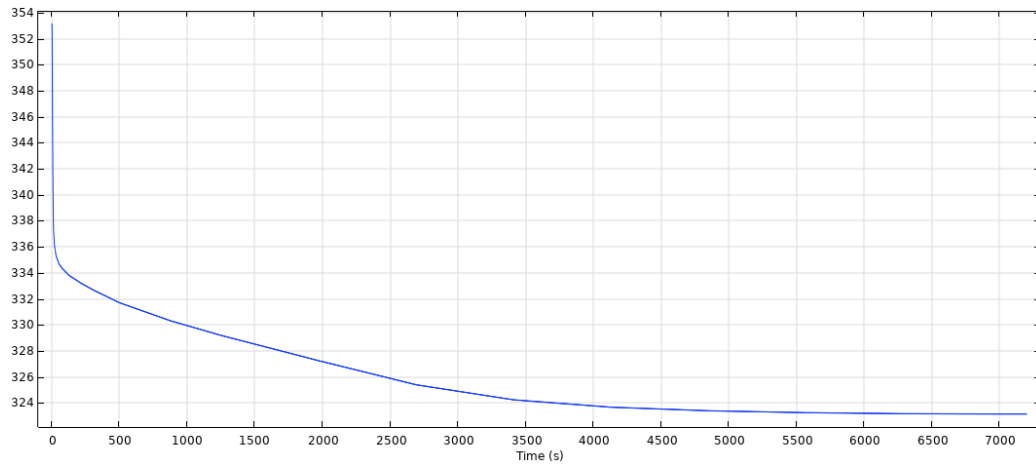


Figure 3.11: Average HTF outlet temperature [K]

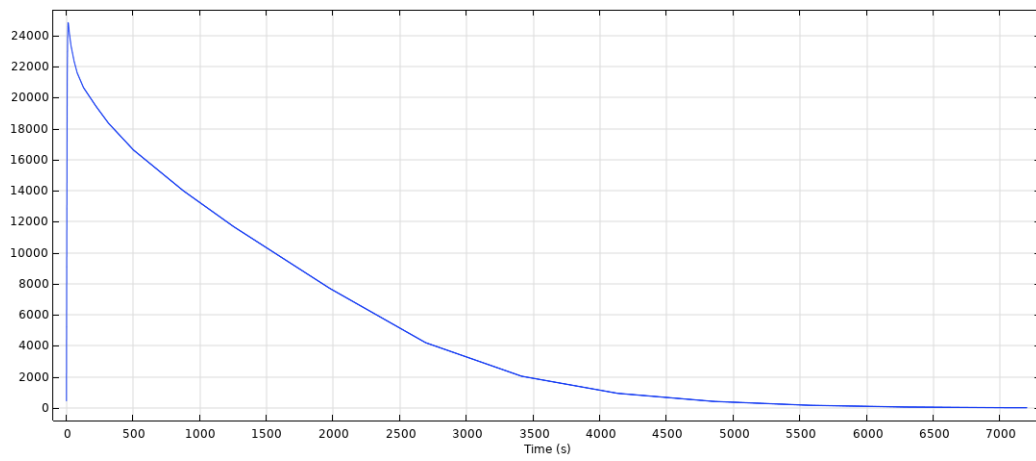


Figure 3.12: Average heat flux [W/m²]

- Salt hydrate, circular fins:

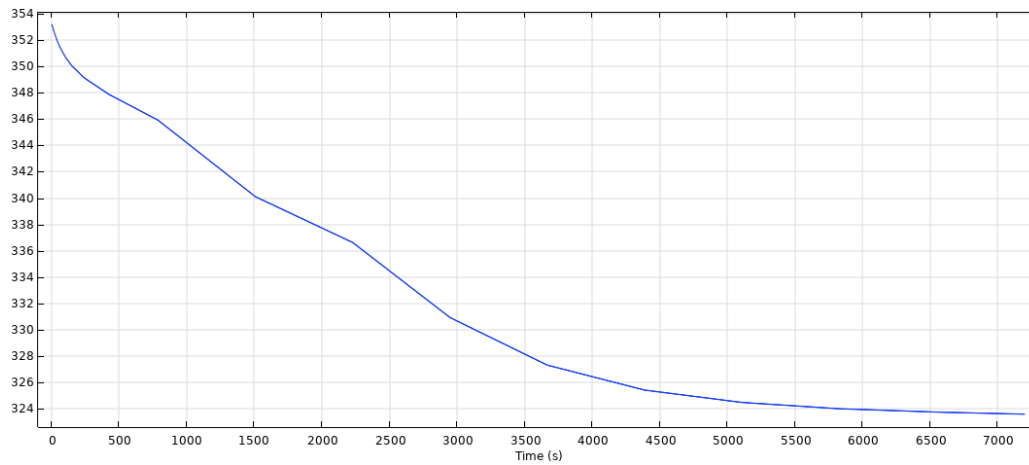


Figure 3.13: Average PCM temperature [K]

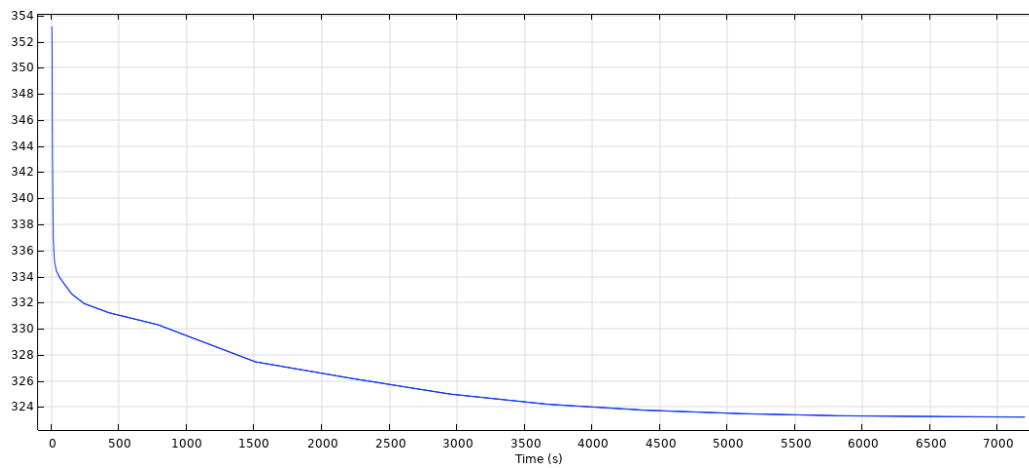


Figure 3.14: Average HTF outlet temperature [K]

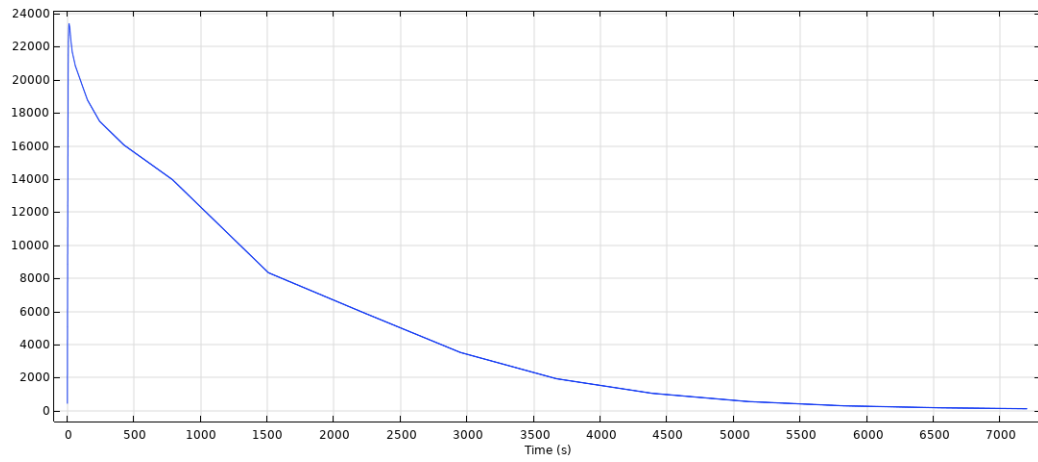


Figure 3.15: Average heat flux [W/m²]

Chapter 4

One-dimensional LHTES model

This chapter main objective is the description of the developed one-dimensional LHTES model whose purpose is the simulation of the behaviour of different shell-and-tube LHTES units from a system perspective. The focus of this model is on low computational effort. The model is based on a-priori known physical and geometrical parameters, thus the formulation is quite general and potentially it can be used during the design phase, but also during the operational phase of the studied LHTES [7]. Most of the work that is described in this chapter is inspired by the work done by A. Colangelo in his PhD thesis [7].

Section 4.1 provides an overview on the main MATLAB characteristics.

Section 4.2 gives an overview on the adopted methodology. The modelling strategy is here explained.

Section 4.3 summarises the features of the one-dimensional pure advection model for the HTF pipe sub-domain. The boundary conditions and the model hypotheses are also defined here.

Section 4.4 precisely describes the analytical modelling approach adopted to represent the dynamic behaviour of the PCM-HCM assembly sub-domain. The thermal power characteristic curve for LHTES heat transfer is identified.

Section 4.5 describes how the two models described in the previous two sections are coupled in order to simulate the behaviour of a LHTES from a system point of view. The model is solved through a MATLAB script.

4.1 Brief overview on MATLAB

The one-dimensional model is developed using the software MATLAB R2022b. MATLAB is a programming and numeric computing platform used in academia, engineering, and industry to analyze data, develop algorithms, and create models. It combines a desktop environment tuned for iterative analysis and design processes with a programming language that expresses matrix and array mathematics directly. MATLAB has many capabilities, but the ones that are of major interest for the development of the model are the possibility to create scripts, functions, and classes (i.e. programming), visualize and explore data through the creation of graphics, data analysis and the possibility to extract data from other softwares like COMSOL Multiphysics.

4.2 Methodology

The integration of LHTES in thermal and multi-energy systems could be made easier through the implementation of faster models able to simulate the behaviour of the LHTES unit. In this thesis is reported a model which describes the behaviour of a shell-and-tube LHTES heat exchanger. This methodology is quite the opposite of what can be seen in the literature (already examined in Chapter 2) in terms of computational time, indeed the latter are quite resource-expensive. The main goal for the model though is the same that characterises the more complex ones, i.e. the outputs of interest are: the outlet temperature of the HTF; the heat flux exchanged at the interface HTF-assembly (PCM and HCM) given the HTF inlet mass flow rate and temperature; the state of charge (SOC) of the LHTES unit.

Predictive models for steady state heat exchangers are widely known and simple. The most well known are the effectiveness number of transfer units method and the logarithmic mean temperature difference method. The drawback of these models though is given by the fact that they cannot be used to study the LHTES units because of the intrinsic transient behaviour of the latter [7].

The methodology adopted in this thesis studies the two sub-domains separately, the HTF sub-domain and the assembly of HCM and PCM sub-domain. The HTF flows inside the LHTES pipes and usually the used fluid coincides

with the fluid flowing inside the hydronic heating system to which the LHTES unit is connected. The HCM-PCM assembly sub-domain instead represents the rest of the LHTES unit, i.e. the pipes and fins materials, as well as the material used to store the thermal energy. Studying the two sub-domains separately it is possible to decouple the heat flux at the interface [7]. More precisely the two sub-domains are modelled as:

- HTF: one-dimensional pure advection numerical model along the axial pipe direction (see Section 4.3);
- Assembly: the transient behaviour of this sub-domain is modelled using analytical thermal power characteristic curves based on the considered LHTES thermo-physical and geometrical parameters (see Section 4.4).

The heat transfer rate exchanged from the HCM-PCM assembly towards the HTF at any time instant mainly depends on the following three parameters [7]: the equilibrium temperature at the contact wall (T_{wall}), the current state of charge of the storage and the conditions at the beginning of the discharging phase. This means that at any time instant the heat flux can be computed and consequently every output that is requested (HTF outlet temperature, SOC and heat flux at the contact wall) can be computed and their time evolution evaluated. It is important to specify that the models are studied under the assumption that the LHTES is experiencing the discharging phase, but the proposed methodology should work fine also for the charging phase. This choice is related to the main objective of the thesis.

4.3 Model for the HTF domain

In this section the model for the heat transfer fluid sub-domain is going to be discussed. A one-dimensional model is adopted along the axial direction of the LHTES pipe. The fluid used for the HTF is water, which is usually the chosen fluid in hydronic heating systems. Considering the thermal properties of the fluid, the heat conduction in the axial direction is considerably smaller than the mass transport. This can be ascribed to the velocity u of the HTF in usual operations, indeed the ratio uL/α (where α is the thermal diffusivity of the HTF and L is the length of the pipe) is much greater than 1 [7]. Eq. 4.1 models the 1D pure advection problem at each time instant for the HTF

along the axial direction:

$$\frac{\partial T(z, t)}{\partial t} + u \frac{\partial T(z, t)}{\partial z} = \frac{1}{\rho_{HTF} c_{p,HTF}} q'''(z, t) \quad (4.1)$$

where z is the coordinate along the pipe axial direction, ρ_{HTF} is the HTF density [kg/m^3]; $c_{p,HTF}$ is the HTF specific heat capacity [$J/(kgK)$] and $q'''(z, t)$ is the volumetric heat generation rate [W/m^3]. The HTF density and specific heat capacity are considered independent of the HTF temperature as simplifying assumptions [7].

Let's move on to the boundary conditions. For the inlet boundary conditions, both velocity and temperature are fixed at each time instant (Dirichlet boundary conditions); this is typical of applications in hydronic heating systems where the inlet conditions are fully known since both temperature and mass flow rate come from the radiators return line (during the discharging phase) or from the boiler supply line (during the charging phase) [7]. At the pipe outlet instead we have an adiabatic boundary condition (Neumann boundary condition) which is given by the following expression:

$$\left. \frac{\partial T}{\partial z} \right|_{z=L} = 0 \quad (4.2)$$

This is a typical condition when modelling this type of problems.

Considering the discretization scheme used for Eq. 4.1, a finite volume approach is used so that the energy is conserved in each section of the pipe. This means that the volumetric heat generation rate can be calculated from the thermal power generated by the corresponding axial section of the assembly when a specific T_{wall} is reached at the interface (as shown in Eq. 4.3) [7].

$$q'''(z, t) = \frac{q_{PCM-HCM}(T_{wall}, SOC, SOC_0)}{A_{pipe} \Delta z} \quad (4.3)$$

where $q_{PCM-HCM}$ is the thermal power incoming from the PCM-HCM assembly [W], $T_{wall}(z, t)$ is the temperature at the contact wall between the HTF domain and the assembly domain; $SOC(z, t)$ is the state of charge of each axial volume of PCM-HCM assembly; SOC_0 is the initial state of charge of the assembly.

T_{wall} is the key element that guarantees that the same heat flux is exchanged in both the HTF and PCM-HCM assembly sub-domains at each

time-step. More details on the heat transfer rate generated by the assembly are available in the following section.

Finally, the advective heat flux between two consecutive cells is determined using an upwind differencing scheme, whereas the time formulation is implicit. The space discretization interval Δz is set to 0.01 m, while the adopted time-step is 1 s. Both of them proved to be good choices since they give results that are independent on the adopted spatial and temporal discretization schemes.

4.4 Thermal power characteristic curves for LHTES heat transfer rate

As already mentioned in the previous section, the term related to q''' (in Eq. 4.1) for this domain depends on the heat transfer rate $q_{PCM-HCM}$ that the quantity of PCM-HCM associated to each pipe is able to release (or absorb depending on the studied phase, i.e. discharge or charge). Now, what has to be evaluated is the most suitable function available to describe the heat transfer rate $q_{PCM-HCM}$.

The time performance of a LHTES is not constant because of the way it stores energy, that is through the change of phase of the PCM. In fact, the rate at which the PCM releases (or absorbs) thermal energy is decreasing in time. This is related to the resistive solid (or liquid) PCM layer that is gradually formed around the fins and HTF pipe as the discharging (or charging) phase proceeds [7]. What follows is that the energy content of the PCM is saturated as time goes on. It is important to state that this saturation process is typical of all storage devices.

The PCM energy saturation process can be modeled using a suitable cumulative distribution function (CDF) [7]. More specifically, looking at the discharging phase, the energy that the LHTES unit releases in time ($E_d(t)$) varies between zero and a maximum value, which is a function of the specific situation under analysis. This maximum value is exactly the amount of energy stored in the LHTES at the beginning of the discharging phase (ΔE_{tot}). In order to describe the energy saturation process in an easier way, the discharged energy can be normalized with respect to the LHTES energy

content (what we obtain is the normalized energy $E_{d,n}$) [7]. This quantity now increases between 0 and 1 and the slope of the curve can be seen in Figure 4.1. The slope of the curve generally depends on three variables: the LHTES design, the operating boundary conditions and the initial conditions. As suggested by A. Colangelo [7], the cumulative function for the Weibull distribution can be used to model such phenomenon:

$$E_{d,n}(t) = \frac{E_d(t)}{\Delta E_{tot}} = 1 - \exp \left[- \left(\frac{t}{\tau_0} \right)^\beta \right] \quad (4.4)$$

This formulation offers the main advantage of needing to define only two parameters: the scale factor τ_0 and the shape factor β . The following subsections are going to better describe such parameters and how they can be defined using only thermal and geometrical variables.

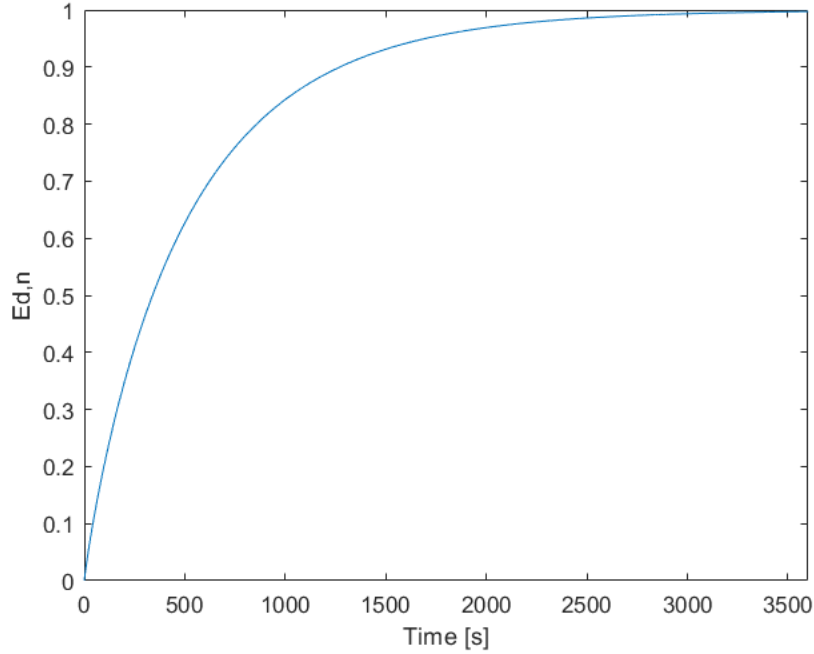


Figure 4.1: Example of normalized discharge energy over time

An expression for the heat transfer rate should be defined in order to link the models for the two sub-domains. The PCM-HCM assembly releases a

thermal power at each time instant that corresponds to the time derivative of Eq. 4.4 [7]. This means that also the thermal power released by the assembly $q_{LHTES}(t)$ is a function of the two factors τ_0 and β :

$$q_{LHTES}(t) = \Delta E_{tot} \frac{dE_{d,n}}{dt} = \Delta E_{tot} \frac{\beta}{\tau_0} \left(\frac{t}{\tau_0}\right)^{\beta-1} \exp\left[-\left(\frac{t}{\tau_0}\right)^\beta\right] \quad (4.5)$$

As A. Colangelo [7] pointed out, such expression is not convenient for the computation of the heat rate released by the PCM-HCM assembly towards the HTF since the independent variable in this expression is time. This could work only if the LHTES is operated under the same inlet boundary conditions. What happens in reality though, is that such boundary conditions may change during the discharging (or charging) process. A more general formulation is hence needed and a change of variable is performed; we want to relate the thermal power to the current state of charge (SOC) [7]. Firstly, the mathematical expression for the SOC is defined (see Eq. 4.6); this comes from Eq. 4.4. Secondly, the time variable is made explicit from Eq. 4.6. Lastly, substitute Eq. 4.7 into Eq. 4.5, this gives the needed expression for the thermal power (see Eq. 4.8):

$$SOC(t) = \exp\left[-\left(\frac{t}{\tau_0}\right)^\beta\right] \quad (4.6)$$

$$t = \tau_0 \left[\ln\left(\frac{1}{SOC}\right)\right]^{\frac{1}{\beta}} \quad (4.7)$$

$$q_{LHTES} = \Delta E_{tot} \frac{\beta SOC}{\tau_0(T_{wall}, SOC_0)} \left[\ln\left(\frac{1}{SOC}\right)\right]^{\frac{\beta-1}{\beta}} \quad (4.8)$$

Since in this equation it appears a logarithm, it must be specified that the argument, i.e. the SOC, has to be greater than 0 (ideally what we have is $0 \leq SOC \leq 1$). The SOC could be null in theory, but in reality this situation almost never happens. It is safe to say then that this constraint is not a problem. As demonstrated by [7] through a few experimental tests, the last 10-15% of the LHTES total energy content either requires a very long time-span to be recovered or it is released at low temperature. It is then possible to state that its practical value is quite debatable.

The expression in Eq. 4.8 corresponds to a family of functions that can be referred to as thermal power characteristic curves [7]. This is due to the fact

that the parameter τ_0 is actually dependent on the temperature at the contact wall (T_{wall}) and the state of charge at the beginning of the process (SOC_0). Thermal power characteristic curves describe the behaviour of a LHTES heat exchanger characterised by a specific design and boundary conditions. To do so, the τ_0 and β factors need to be properly defined.

4.4.1 Derivation of the time constant τ_0

The scale factor τ_0 from the dimensional point of view is a time, so it is appropriate to call it a time constant. By definition, τ_0 represents the time needed by the PCM-HCM assembly to release 63.2% of its total energy content [7]:

$$E_{d,n}(\tau_0) = \frac{E_d(\tau_0)}{\Delta E_{tot}} = 0.632 \quad (4.9)$$

This means that this scale factor identifies how fast the discharging process is; the lower its value, the faster is the discharging process. It has been demonstrated in the literature that the speed of discharge is dependent on the specific LHTES boundary conditions and design [7, 87]. It is then reasonable to state that the time constant should be a function of such factors.

The total energy stored in the LHTES ΔE_{tot} is the sum of the initial energy content of the entire domain (see Eq. 4.10). The sensible energy of the HCM and the sensible plus latent energy of the PCM are evaluated between the homogeneous initial temperature T_0 and the the minimum temperature at which it can be ideally cool down, i.e. the contact wall temperature T_{wall} . All these terms can be computed from the thermo-physical parameters of the interested materials, but the initial state of charge SOC_0 is the only missing factor. However, in most of the real scenarios, SOC_0 assumes values which are comprised in the interval 0.95 - 1, so also this parameter is actually available [7]. It must be noted that even if the range of choice seems limited, the methodology herein proposed does not exclude the possibility to choose values which are lower (but in any case greater than 0).

$$\Delta E_{tot} = \rho_{PCM} V_{PCM} SOC_0 \left[\int_{T_{wall}}^{T_0} c_p dT + \Delta h_{lat} \right] \quad (4.10)$$

The energy discharged after the time interval τ_0 ($E_d(\tau_0)$) is estimated through the definition of an average heat rate q_{avg} released by the assembly

towards the HTF within that time frame [7]:

$$E_d(\tau_0) = q_{avg}\tau_0 \quad (4.11)$$

Particular attention must be paid to the definition of the average heat flux since it requires some approximations. During the LHTES discharging process heat is discharged mainly by conduction, apart from a short initial interval (the transitory) where the natural convection is quite appreciable [89]. The conductive mechanism is particularly important, especially when dealing with compact designs like the one in which longitudinal fins are used. Additionally, the PCM thermal resistance is far greater than the one of the pipe and fins. For these reasons the average heat flux during the time span τ_0 can be approximated by the conductive heat flux across a PCM layer of thickness l_c , where l_c is an estimate for the average PCM layer around the HCM [7]. Thus, it depends on the LHTES heat exchanger design. The characteristic length l_c is given by the following expression [7]:

$$l_c = \frac{V_{PCM}}{A_{contact}} \quad (4.12)$$

where $A_{contact}$ is the total contact area between the PCM and the HCM fins. Concerning the driving temperature difference, the temperatures that are of interest in the first half of the discharging process are T_{wall} and T_0 .

$$q_{avg} = \frac{k_{PCM}}{l_c} A_{contact} (T_0 - T_{wall}) \quad (4.13)$$

Now it is possible to substitute Eq. 4.13 into Eq. 4.11, then substitute this together with Eq. 4.10 into Eq. 4.9. The result of all these passages is showed in the following equation:

$$\tau_0 = 0.632 \frac{\rho_{PCM} l_c^2 SOC_0 \left[\int_{T_{wall}}^{T_0} c_p dT + \Delta h_{lat} \right]}{k_{PCM} (T_0 - T_{wall})} \quad (4.14)$$

Hence, the following are the main parameters needed to define τ_0 :

- the geometrical characteristics of the LHTES unit (l_c);
- the initial PCM state (T_0 and SOC_0);
- the contact wall temperature T_{wall} .

The first two parameters are already available, the only unknown is the temperature T_{wall} , so the thermal power released by the PCM-HCM assembly towards the HTF at each time step can be estimated only as a function of such temperature. Note that the other independent variable in Eq. 4.8 is the SOC, but this one is actually known at the beginning of each simulation time step [7].

It must be specified that such definition for τ_0 is valid only if the initial PCM condition is homogeneous [7]. This condition may not be always satisfied in real applications, i.e. when the LHTES unit is partially charged and then immediately discharged; in this situation only a smaller thickness of PCM is liquid around the LHTES fins. Regions distant from the fins instead remain solid. In such situation, the initial state of charge (SOC_0) will be much lower than 1, resulting in a reduced time constant. Also the PCM characteristic length l_c is deemed to be reduced. Therefore, an additional factor multiplying l_c in Eq. 4.14 could be introduced to account for non-homogeneous PCM initial conditions [7].

Note: this expression for τ_0 is going to be modified in Section 5.2 in order to achieve a better accuracy with the three-dimensional model.

4.4.2 Derivation of the shape factor β

As the name suggests, the shape factor β affects the shape of the thermal power curve. This factor has to assume a value which is at maximum equal to 1. This condition has to be respected in order to have a monotonically decreasing trend with respect to time. If instead is assigned to β a value larger than 1, then the discharged thermal power curve would present an inflection point, which is not reasonable [7]. The shape factor affects mostly the second part of the curve since it affects the final time at which the LHTES energy content is fully released. This can be seen in Figure 4.2.

According to A. Colangelo's intuition [7], which resulted to be mostly correct, the value of β depends on the proportion between PCM and HCM in the LHTES heat exchanger. This can be partially explained by the fact that the HCM mass speeds up the discharging process because of the higher thermal conductivity. Indeed, the difference with the PCM thermal conductivity is of multiple orders of magnitude, the latter being of course the lowest. The

effect of slowing down the discharging process is also expected to be more evident in the last phase of the process since it becomes more difficult to extract energy from the PCM mass as a solid PCM layer thickens between the pipe and the farthest PCM region [7]. For this reason β is expected to be influenced by the weight of HCM mass on the overall assembly mass. The following expression for the shape factor is given in [7]:

$$\beta = \frac{M_{PCM}}{M_{PCM} + M_{HCM}} \quad (4.15)$$

The value of the shape factor defined in this way is only dependent on the LHTES composition, hence it is constant in time.

Note: this expression for β is going to be modified in Section 5.2 in order to achieve a better accuracy with the three-dimensional model.

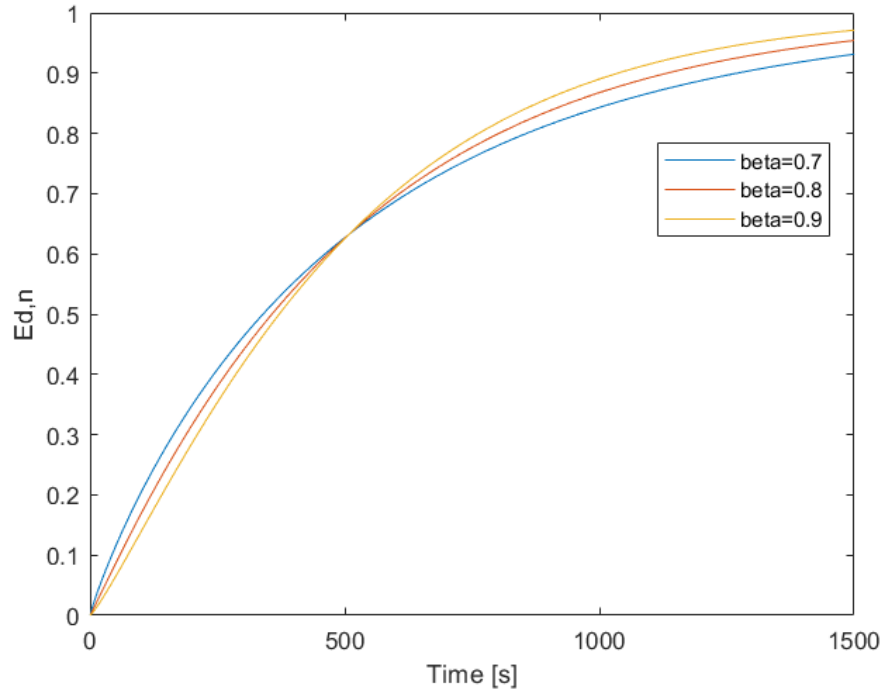


Figure 4.2: Effect of different β values on the normalized discharged energy

4.5 Model solution algorithm

This section describes how the two models, discussed in the previous two sections, are coupled in order to simulate the behaviour of a LHTES from a system point of view. The problem expressed in Eq. 4.1 is solved thanks to a MATLAB script. The algorithm's structure is inspired by the one developed by A. Colangelo [7].

For the first step, it is needed to define the geometrical characteristics of the LHTES unit, as well as the thermo-physical properties of the different materials under analysis (HTF, HCM and PCM).

The second step consists in computing the PCM characteristic length l_c and the shape factor β accordingly to Eq. 4.12 and Eq. 4.15 respectively.

The following step is the definition of the LHTES energy content function. An ideal discharge ending condition at each time-step is allowed to be set in this way [7]. In fact, the total amount of energy that can be released by the LHTES unit depends on the inlet HTF temperature because of the PCM sensible energy content. Ideally, the LHTES unit is fully discharged when the PCM temperature is in equilibrium with the HTF inlet temperature.

For the fourth step, the one-dimensional finite volume problem formulation, shown in Eq. 4.16, has to be solved at each time-step. The HTF domain is discretized in small intervals of length Δz . The value for Δz is set to 0.01m. Then, the problem matrix A and the right-hand-side vector b are built considering also the boundary conditions. The discretized version of the problem creates a sparse matrix A , which has to be built using the "spdiags" command to optimise the memory allocation and the speed of computation. The initial conditions are then defined (T_0 , SOC_0 and the initial energy content of the LHTES). Before moving to the next step of the solution algorithm, the output variable have to be initialized (HTF outlet temperature, heat transfer rate and SOC).

$$A^n \cdot T_{HTF}^n = b^n \quad (4.16)$$

The fifth step involves the definition of the reference quantities ΔE_{ref} , τ_{ref} and q_{ref} . These three quantities are needed to linearize the problem solution in the following steps [7]. They are evaluated accordingly to Eq. 4.10, Eq. 4.14 and Eq. 4.8 respectively, by setting T_{wall} to a reference temperature T_{ref}

equal to 20°C. The choice of the reference temperature is quite free, the only constraint it has to respect is to be much lower than the PCM solidification temperature [7].

After all these steps, it is finally possible to compute the HTF temperature distribution along the domain at each time-step n ($T_{HTF,j}^n$) thanks to a cyclic procedure. The objective of the loop is to find a solution to Eq. 4.16 at each time-step. To do so, the inner terms of b must be evaluated at each time-step because they depend on the thermal power exchanged between the two sub-domains (HTF and PCM-HCM assembly) [7]. Firstly, the temperature at the interface $T_{wall,j}^n$ is computed considering that the relationship between $q_{wall,j}^n$ and $T_{wall,j}^n$ is linear when the SOC is fixed, i.e. at each time-step [7]. The thermal power exchanged at the contact wall $q_{wall,j}^n$ is expressed through Eq. 4.17 by imposing an a-priori reference value, i.e. q_{ref} [7].

$$q_{wall,j}^n = q_{ref} - q_{ref} \frac{T_{wall,j}^n - T_{ref}}{T_0 - T_{ref}} \quad (4.17)$$

A graphical representation of Eq. 4.17 is shown in Figure 4.3.

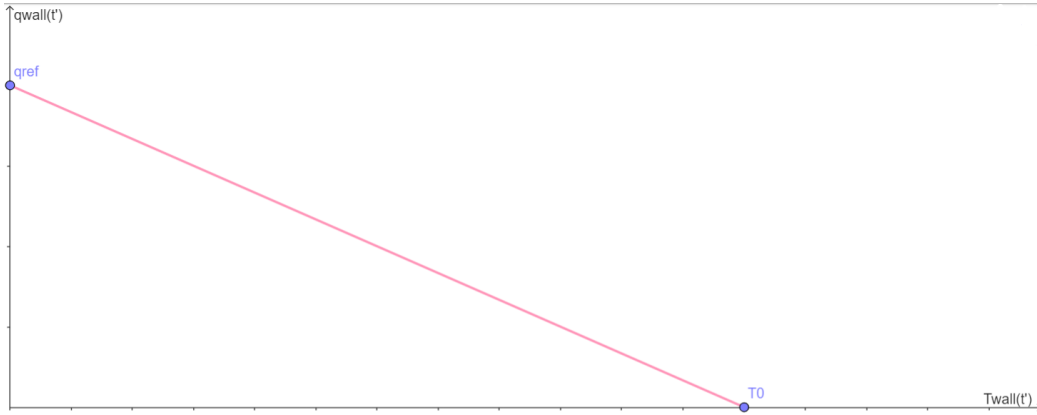


Figure 4.3: Linearization of the heat rate exchanged at the contact wall

However, the heat rate at the contact wall can also be expressed considering the HTF sub-domain accordingly to Eq. 4.18. Now, the driving temperature difference is assessed as a function of the HTF axial temperature at the previous time-step ($T_{HTF,j}^{n-1}$), so that an implicit iterative procedure is avoided, which could lead to instabilities in the algorithm [7].

$$q_{wall,j}^n = h_{conv} A_{lat,j} (T_{wall,j}^n - T_{HTF,j}^{n-1}) \quad (4.18)$$

Looking at Eq. 4.18, h_{conv} represents the heat transfer coefficient and $A_{lat,j}$ represents the lateral external surface of each HTF pipe discretized volume.

Now, by combining Eq. 4.17 and Eq. 4.18, $T_{wall,j}^n$ can be evaluated at the beginning of each time-step using the following equation:

$$T_{wall,j}^n = \frac{q_{ref} - \frac{T_{ref}q_{ref}}{T_{ref}-T_0} + h_{conv}A_{lat,j}T_{HTF,j}^{n-1}}{h_{conv}A_{lat,j} - \frac{q_{ref}}{T_{ref}-T_0}} \quad (4.19)$$

Once we have $T_{wall,j}^n$, the thermal power exchanged is computed using Eq. 4.18. The heat transfer coefficient h_{conv} is computed using Eq. 4.20 considering the thermal conductivity of the HTF (k_{HTF}), the pipe inner diameter (d_i) and the Nusselt non-dimensional number (Nu). The latter is estimated through the Dittus-Boelter correlation (Eq. 4.21) when the HTF flow is turbulent or by the correlation for laminar flows with an entry length (Eq. 4.22) when the HTF flow is laminar [90].

$$h_{conv} = \frac{k_{HTF}Nu}{d_i} \quad (4.20)$$

$$Nu = 0.023Re^{4/5}Pr^n \quad \text{with: } n=0.4 \text{ (discharge); } n=0.3 \text{ (charge)} \quad (4.21)$$

$$Nu = 3.66 + \frac{0.0668(d_i/z)RePr}{1 + 0.04((d_i/z)RePr)^{2/3}} \quad (4.22)$$

Now, the inner values of the right-hand-side vector b can be expressed through Eq. 4.23. Eventually, the HTF temperature distribution can be computed solving the linear equation (Eq. 4.16) at each time-step.

$$b_j^n = T_{HTF,j}^{n-1} + \frac{\Delta t}{\rho_{HTF}c_{p,HTF}A_{lat,j}\Delta z}q_{wall,j}^n \quad (4.23)$$

Before exiting the loop, the output variables of interest are stored. These consist of:

- the HTF outlet temperature (i.e. the last value of $T_{HTF,j}^n$);
- the total LHTES heat transfer rate, which is computed as:

$$q_{tot,LHTES}^n = n_{pipes} \sum q_{wall,j}^n \quad (4.24)$$

- the LHTES state of charge SOC^n , which is computed as the average state of charge of all the PCM-HCM assembly small volumes associated to each HTF discretized volume.

Before moving to the next iteration, several quantities are updated. These are:

- the total LHTES energy content;
- the LHTES SOC;
- the HTF temperature distribution.

If there are changes to be applied to the inlet conditions (e.g. the inlet temperature, the inlet mass flow rate and consequently the heat transfer coefficient), this is the moment (if needed) [7]. Also the values inside the problem matrix A and the right-hand-side vector b have to be changed if any modification is applied.

The MATLAB script of the discussed one-dimensional model is available at the following online repository [91].

Chapter 5

Models comparison

This chapter compares the results between the one-dimensional dynamic model and the three-dimensional numerical model for the LHTES heat exchangers studied in the previous chapters. This comparison is needed to find a suitable way to increase the accuracy for the one-dimensional dynamic model through the introduction of a few correcting parameters. Also, understanding the gains in terms of computational time given by the one-dimensional model is an important goal of this chapter. The quantities of interest that are analyzed are the time evolution of the HTF outlet temperature and the LHTES state of charge. To make the comparison work, the same boundary and initial conditions are applied. The initial condition is represented by a fully charged LHTES unit ($SOC_0 = 1$), i.e. the whole LHTES domain is set to an initial temperature equal to 80°C. For the HTF inlet boundary conditions, these are the inlet temperature set to 50°C and the inlet mass flow rate equal to 0.03kg/s, resulting in a Reynolds number $Re=5915$, i.e. turbulent flow condition.

Section 5.1 shows the results obtained by the one-dimensional model described in the previous chapter and compares it with the ones of the three-dimensional model.

Section 5.2 describes the adopted reasoning on how the correcting parameters are found.

Section 5.3 shows the final results obtained after implementing the correcting factors inside the one-dimensional model and compares the results with the ones of the three-dimensional model.

5.1 First comparison

A first comparison of the results obtained from the one-dimensional dynamic model and the three-dimensional model is needed to gain useful insights on the simplified model's performance. As can be seen from Figure 5.1 - 5.4, the one-dimensional model appears to be quite accurate when considering the HTF outlet temperature, but a noticeable difference is visible from Figure 5.5 - 5.8, i.e. when comparing the SOC.

- HTF outlet temperature:

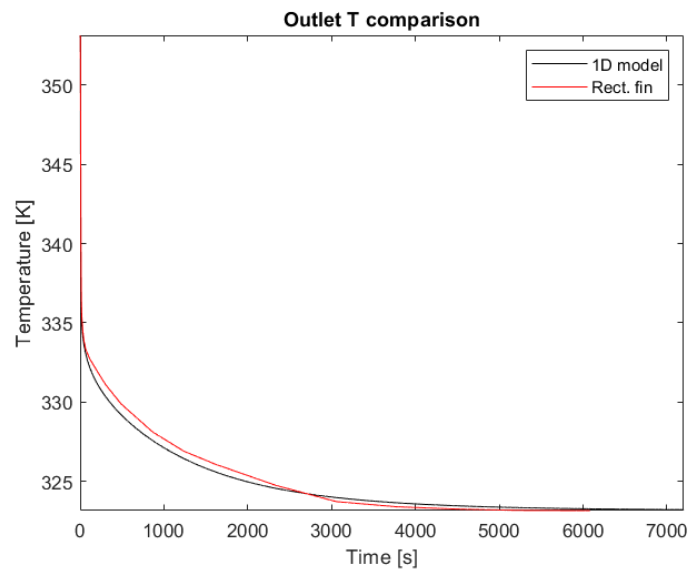


Figure 5.1: Paraffin, longitudinal fins

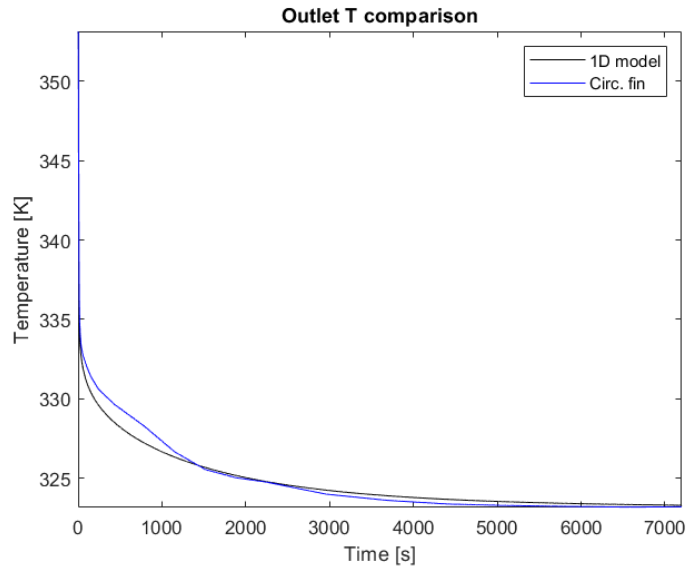


Figure 5.2: Paraffin, circular fins

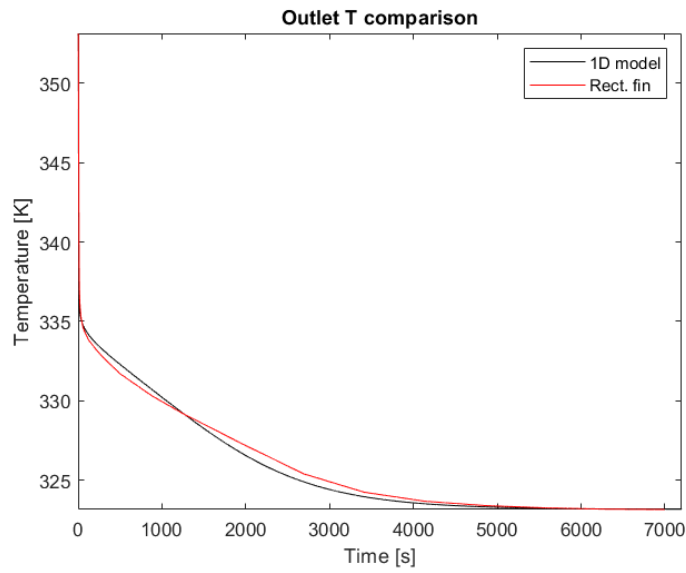


Figure 5.3: Salt hydrate, longitudinal fins

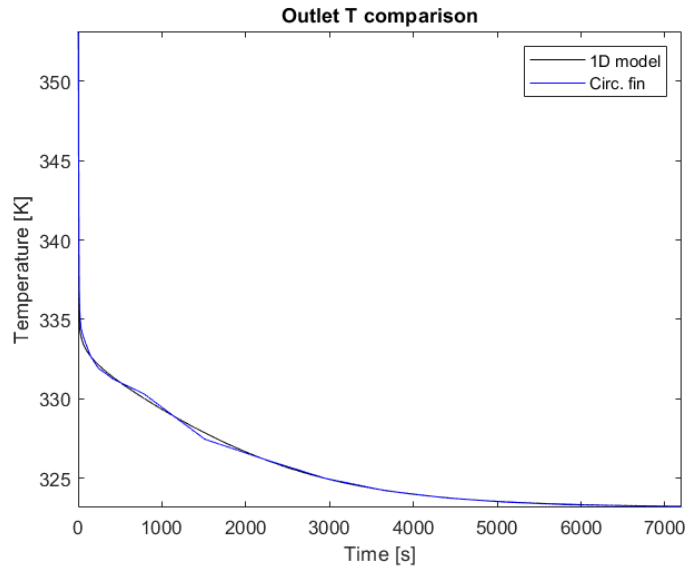


Figure 5.4: Salt hydrate, circular fins

- LHTES state of charge:

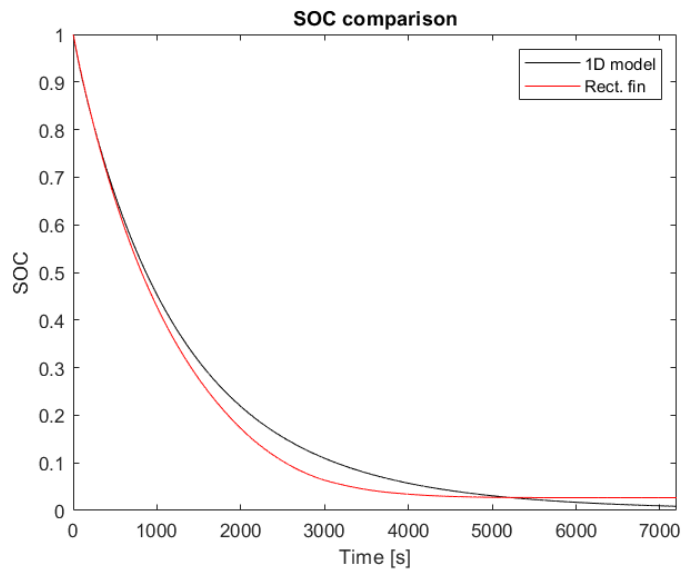


Figure 5.5: Paraffin, longitudinal fins

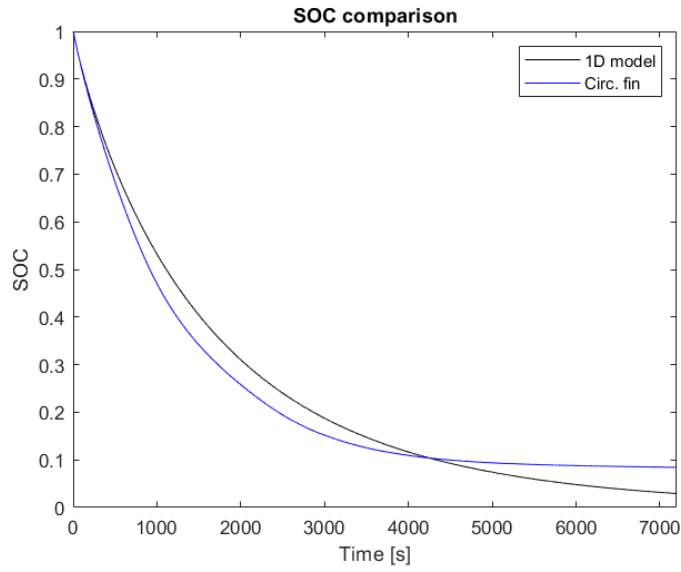


Figure 5.6: Paraffin, circular fins

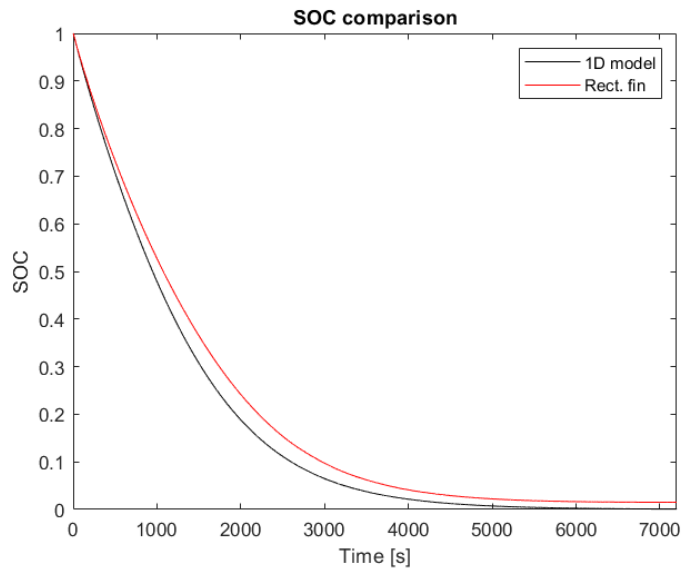


Figure 5.7: Salt hydrate, longitudinal fins

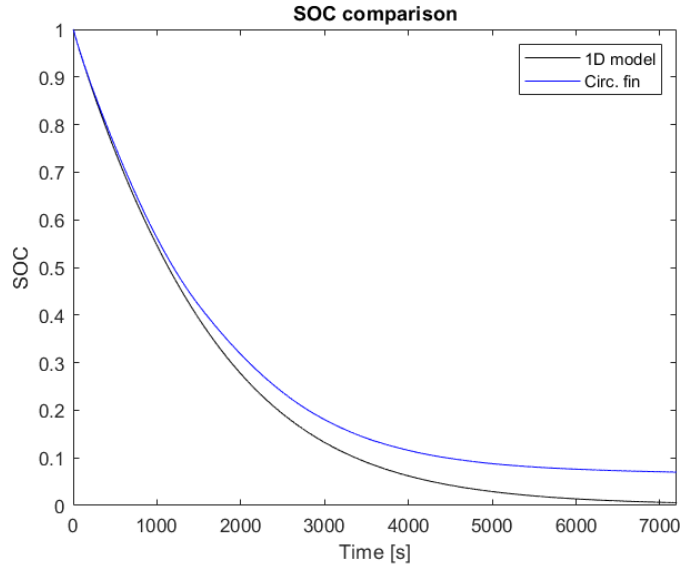


Figure 5.8: Salt hydrate, circular fins

5.2 Correcting parameters

So, as is shown in Figure 5.5 - 5.8, the trend for the SOC computed according to the three-dimensional models and the one from the one-dimensional models is quite different, especially at the end of the discharging process, where the one-dimensional model seems to struggle in assessing the energy dissipated in the areas farthest from the fins. Also the one-dimensional model overestimates the SOC at the end of the useful discharging process for the paraffin PCM, while, on the opposite, it underestimates the SOC when considering the salt hydrate case.

In order to achieve a better accuracy for the one-dimensional model, a possible solution lies in the introduction of a few correcting parameters into the normalized discharged energy equation (Eq. 4.4). More precisely, the equations used to define the shape factor β and the time constant τ_0 are modified (Eq. 4.14 and Eq. 4.15). The idea is to introduce some non-dimensional correcting factors which pre-multiply the two aforementioned parameters, so that the original model can still be applied while obtaining

more realistic results. Before diving into the final expressions for β and τ_0 , it is necessary to understand and analyse which are the materials and geometric characteristics of interest.

Let's start with the geometric characteristics. If we compare the longitudinal fins model with the one with the circular fins and we look at the trend of the average PCM temperature during the discharging process (see Figure 5.9 and Figure 5.10), it is possible to state that the first one is more efficient than the second one. A typical parameter used when evaluating the fin's effectiveness is the ratio between the fin's area and the fin's perimeter, so it makes sense to consider it when evaluating the discharged energy. Another important parameter that is of interest is the already mentioned characteristic length l_c (Eq. 4.12). Hence the following fin shape factor γ is defined:

$$\gamma = \frac{A_{fin}}{l_c P_{fin}} \quad (5.1)$$

where A_{fin} is the fin contact area, P_{fin} is the fin perimeter.

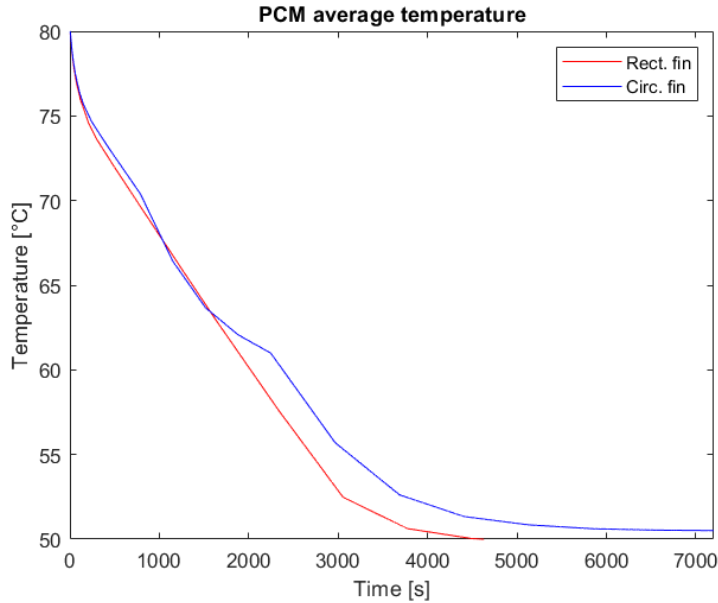


Figure 5.9: Paraffin PCM average temperature

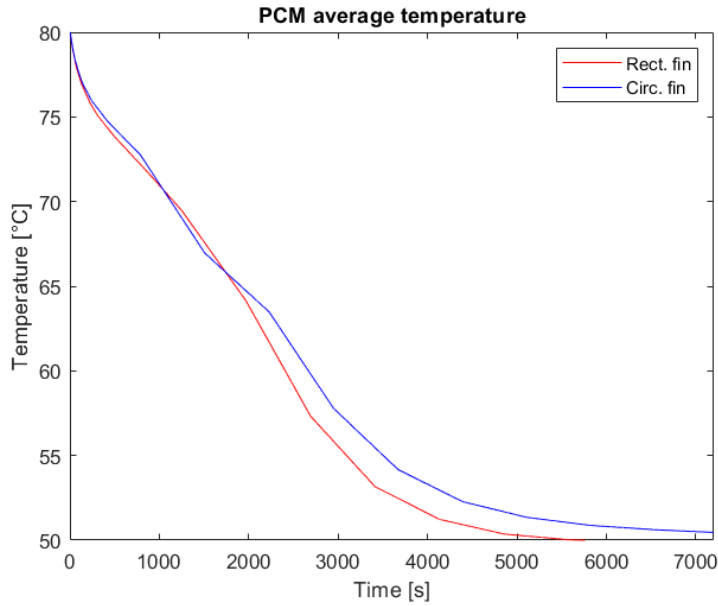


Figure 5.10: Salt hydrate PCM average temperature

Let's move on now to the thermo-physical properties of the materials, most importantly the thermal conductivity of the PCM. As already discussed, the thermal problem can be modeled as a pure conduction problem; this is why it is important to consider such material characteristic. A couple of non-dimensional numbers which take into account the thermal conductivity of the material are the Biot number Bi and the Fourier number Fo (see Eq. 5.2 and eq. 5.3 respectively). The Biot number plays a fundamental role in conduction problems that involve surface convection effects. It provides a measure of the temperature drop in the solid relative to the temperature difference between the surface and the fluid. The Biot number is defined as follows:

$$Bi = \frac{h_{conv}L}{k} \quad (5.2)$$

where h_{conv} is the heat transfer coefficient of the HTF, k is the thermal conductivity of the PCM and L is the ratio of the solid's volume to surface area ($L = V/A$).

The Fourier number provides instead a measure of the relative effectiveness with which a solid conducts and stores thermal energy. It is defined as

follows:

$$Fo = \frac{\alpha\tau_{0,ref}}{L^2} = \frac{k\tau_{0,ref}}{\rho c_{p,s}L^2} \quad (5.3)$$

where ρ is the density of the PCM, $c_{p,s}$ is the specific heat capacity of the solid PCM and $\tau_{0,ref}$ is the time constant evaluated accordingly to Eq. 4.14 using as T_{wall} the reference temperature $T_{ref}=20^\circ\text{C}$.

Now that the parameters of interest are defined, a trial-and-error procedure is followed in order to find the best correcting parameters, so that the superposition of the results obtained for the one-dimensional model and the three-dimensional model results sufficiently accurate. The following corrected expressions for β and τ_0 are found:

$$\beta = \frac{M_{PCM}}{M_{PCM} + M_{HCM}} \left[0.48\gamma \left(\frac{Bi}{Fo} \right)^{\frac{1}{5}} \right] \quad (5.4)$$

$$\tau_0 = 0.632 \frac{\rho_{PCM} l_c^2 SOC_0 \left[\int_{T_{wall}}^{T_0} c_p dT + \Delta h_{lat} \right]}{k_{PCM}(T_0 - T_{wall})} \left[1.3 \left(\frac{Bi}{Fo} \right)^{\frac{1}{3}} \right] \quad (5.5)$$

5.3 Final comparison

A final comparison of the results obtained in the one-dimensional dynamic model and the three-dimensional model is performed. As it can be seen from Figure 5.11 - 5.14, the one-dimensional model still is quite accurate when considering the HTF outlet temperature, but a noticeable improvement is visible from Figure 5.15 - 5.18, i.e. when comparing the SOC. The trend for the SOC computed according to the three-dimensional models and the one from the one-dimensional models is still quite different at the end of the discharging process, where the one-dimensional model seems to struggle in assessing the energy dissipated in the areas farthest from the fins. Anyway this difference is not of interest for the thesis considering that in practice most of the useful energy content of the LHTES has already been released when its state of charge drops below 15-20% (indeed, at this stage the HTF has a temperature increase equal to or even lower than 1°C compared to its

inlet value). Instead when looking at the useful part of the SOC plot (i.e. from 100% to 20%), an almost perfect overlapping is obtained.

- HTF outlet temperature:

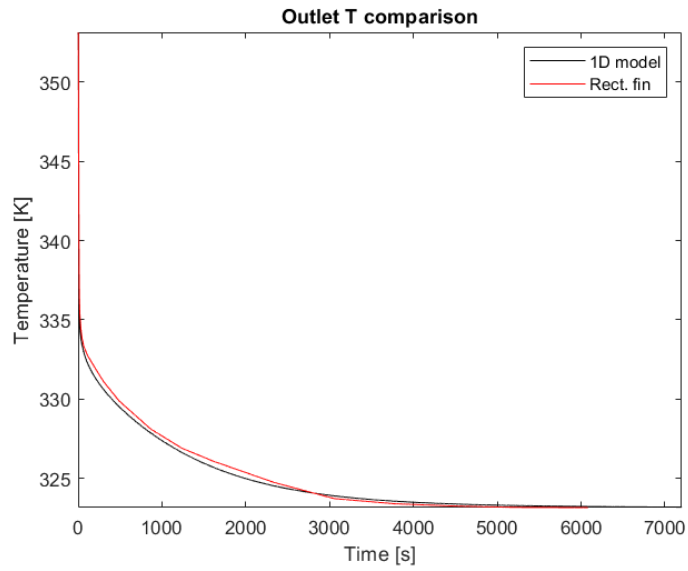


Figure 5.11: Paraffin, longitudinal fins

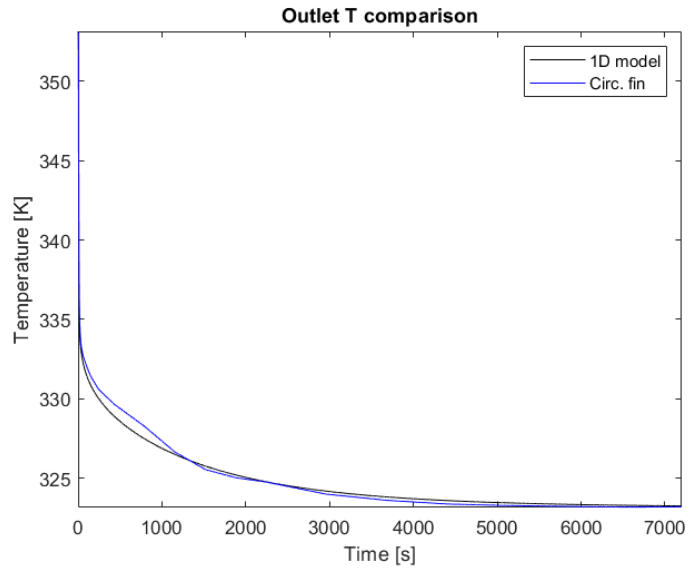


Figure 5.12: Paraffin, circular fins

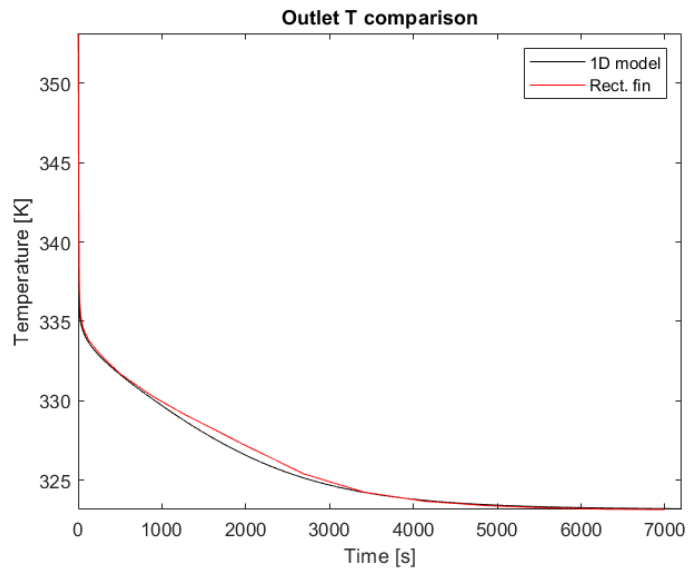


Figure 5.13: Salt hydrate, longitudinal fins

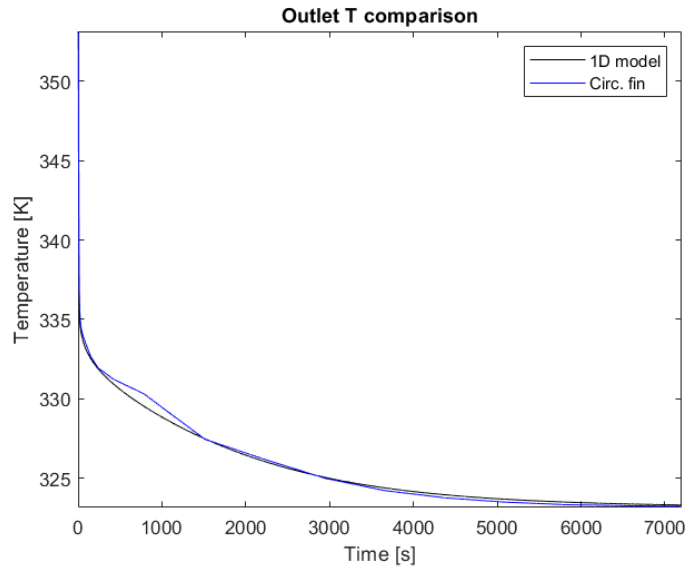


Figure 5.14: Salt hydrate, circular fins

- LHTES state of charge:

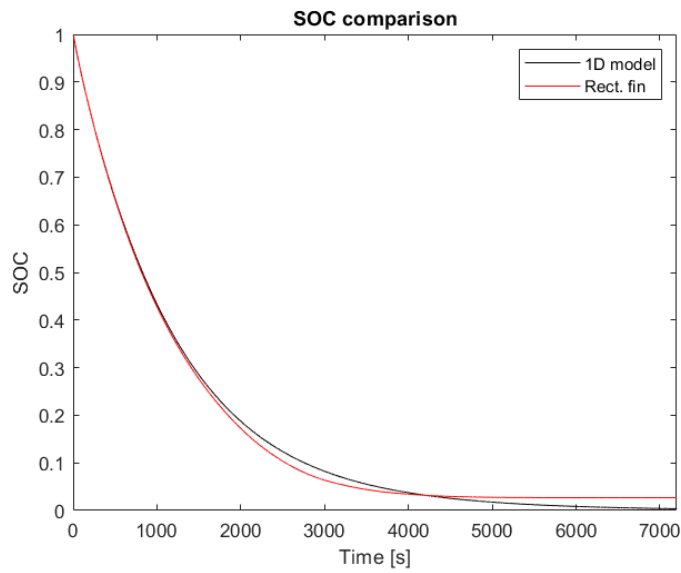


Figure 5.15: Paraffin, longitudinal fins

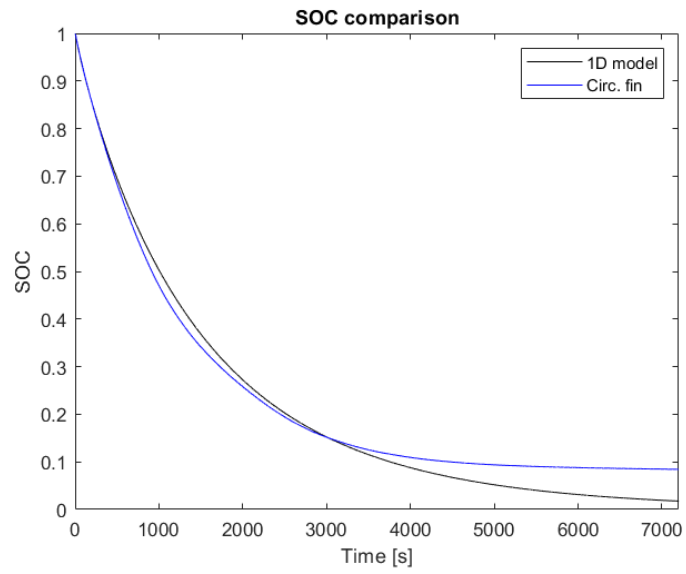


Figure 5.16: Paraffin, circular fins

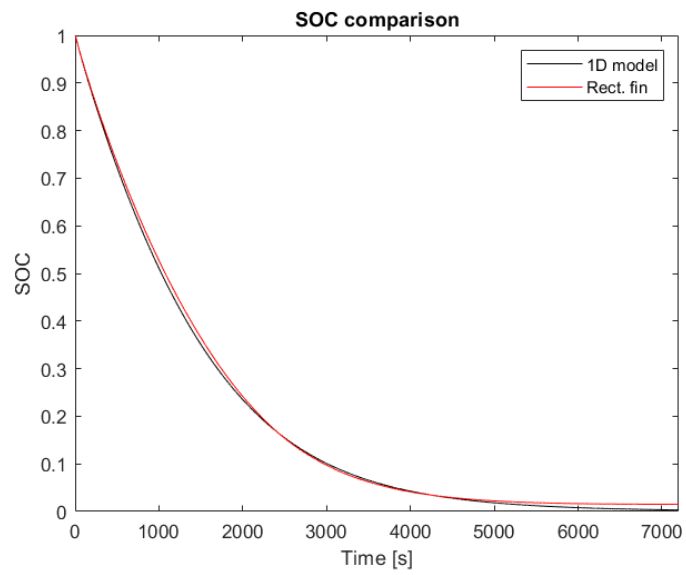


Figure 5.17: Salt hydrate, longitudinal fins

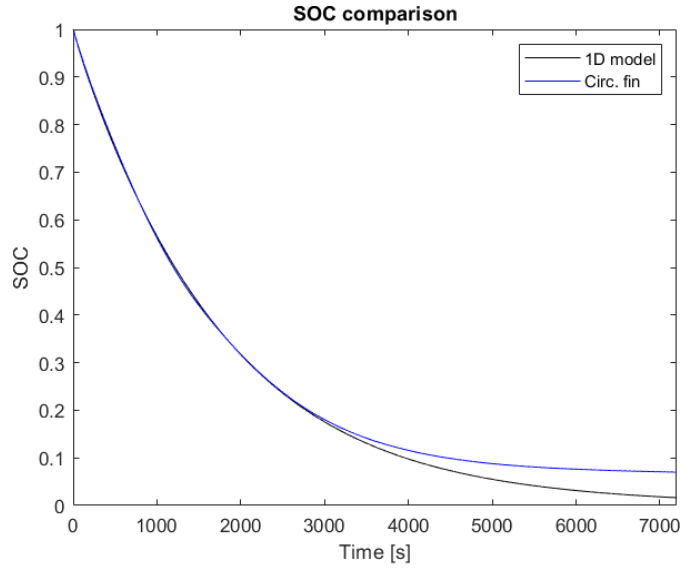


Figure 5.18: Salt hydrate, circular fins

Table 5.1 and Table 5.2 show the average relative error for the HTF outlet temperature and the maximum error for the state of charge for the different models. The results obtained for the HTF outlet temperature are very satisfying since the average relative error is below 1% for every configuration. Also when looking at the maximum deviation from the three-dimensional model, the difference is always lower than 5%, which means that the results are acceptable.

Table 5.1: HTF outlet temperature average relative error

Model	Value
Paraffin, longitudinal fins	0.54%
Paraffin, circular fins	0.54%
Salt hydrate, longitudinal fins	0.58%
Salt hydrate, circular fins	0.41%

Table 5.2: SOC maximum error

Model	Value
Paraffin, longitudinal fins	2.06%
Paraffin, circular fins	3.36%
Salt hydrate, longitudinal fins	1.66%
Salt hydrate, circular fins	1.15%

Now, let's consider the computational time. The presented simulations were implemented in the commercial software MATLAB R2022b (for the one-dimensional model) and COMSOL Multiphysics 6.1 (for the three-dimensional model). The simulations were run on a 4-core CPU (11th Gen Intel i7-1165G7 @2.80GHz, 16GB RAM). The average computational time for the three-dimensional model simulation is about 8h 30min, whereas for the one-dimensional model simulation is about 2s. The advantage for the one-dimensional model is huge when considering the computational time, hence it represents an interesting first step in finding the solution for the LHTES design process.

Chapter 6

Conclusions

This chapter sums up the results obtained in this thesis, focusing on the research main contributions, identifying the limitations and evaluating future perspectives.

6.1 Research contributions

The thesis main contribution is represented by the creation of a fast and accurate one-dimensional dynamic model for system-level simulations of latent heat thermal energy storage units. The modelling approach proved to be very fast and acceptably accurate when introducing the correcting parameters discussed in Section 5.2. It becomes quite interesting when the modeller's objective lies in system-level quantities such as the heat transfer fluid outlet temperature, the LHTES state of charge or the heat transfer rate exchanged in the heat exchanger. All these quantities can be evaluated in a few seconds, achieving results that are comparable with the ones obtained by a three-dimensional model, which instead is much more expensive from the computational time's point of view. The difference in time is remarkable, with a jump in computational time from more than 8 hours to just a few seconds. The discussed modelling approach results to be also appreciably accurate with respect to a three-dimensional model given the same LHTES design characteristics, boundary and initial conditions. More specifically, the average relative error for the HTF outlet temperature results to be lower than 1%, whereas the maximum deviation for the SOC in its useful part is way lower than 5%, which proves the validity of the proposed model, at least from

a simulation's point of view.

Another achievement of the proposed thesis lies in the fact that no experimental calibration parameters are needed. The model relies only on a-priori known geometrical and thermo-physical parameters of fins and phase change material. This gives an additional benefit to the already fast simulation model, since no measurements on site are requested for it to simulate correctly the behaviour of the LHTES heat exchanger.

In this thesis two different fins configurations are tested: the longitudinal one and the circular one. The effect of the fin choice can be analysed with the proposed model, gaining useful information about the effectiveness of said fins, as well as the speed of discharge, by looking at the SOC's trend in time. Looking at said plot, we can also appreciate the difference between different materials used for the PCM; more precisely here are evaluated a specific typology of bio-based paraffin and a salt hydrate as PCMs.

6.2 Limitations and future perspectives

A few limitations can be noted by the author. First, it is clear from the state of charge plots that the developed one-dimensional model is not able to correctly simulate the discharged heat rate at the end of the process since it overestimates it. This can be ascribed to the fact that the model is not able to accurately simulate the behaviour of the PCM regions which are farthest from the fins. Second, only a couple fins design and PCM materials are analysed in this work, hence the accuracy of the proposed model is not confirmed for other design choices. Third, only the discharging process is being studied here, while the charging process is left uncovered. This choice is related to the objective of the thesis, otherwise also the charging process could have been analysed. Last, no experimental analysis has been performed, only a comparison with a more accurate three-dimensional model, so the obtained results can't be proven as correct or wrong in a real heating system.

Even if a few limitations exist, this thesis opens multiple future perspectives. First, the proposed modeling approach can assist in determining the optimal size of LHTES and in evaluating its system-level performance. The former aspect enables customization of the LHTES size to meet specific user requirements during the design phase, while the latter facilitates the analysis

of effective control strategies for LHTEs during the operational phase. This means that multiple optimization problems could be developed according to the modeler's objectives. Second, an experimental campaign focused on both charging and discharging phases should be set up in order to validate the model results. Third, different shell-and-tube internal geometries could be tested to validate the general application of the one-dimensional model. To conclude, this thesis provides precious insights into the simulation field by improving the results obtained by A. Colangelo [7].

References

- [1] International Energy Agency (IEA). *Energy Efficiency 2023*. Tech. rep. 2023.
- [2] International Energy Agency (IEA). *Buildings*. URL: <https://www.iea.org/energy-system/buildings>. (accessed: 2024).
- [3] International Energy Agency (IEA). *Heating*. URL: <https://www.iea.org/energy-system/buildings/heating>. (accessed: 2024).
- [4] International Renewable Energy Agency (IRENA). *Innovation outlook: Thermal energy storage*. Tech. rep. 2020.
- [5] F. Agyenim et al. “A review of materials, heat transfer and phase change problem formulation for latent heat thermal energy storage systems (LHTESS)”. In: *Renewable and Sustainable Energy Reviews* 14.2 (2010), pp. 615–628.
- [6] A. Abd et al. *Material and Component Development for Thermal Energy Storage*. Tech. rep. 2020.
- [7] A. Colangelo. “Fast modelling, realisation and experimental characterisation of innovative latent heat storage units for system integration”. PhD thesis. Politecnico di Torino, 2023.
- [8] B. Cárdenas and N. León. “High temperature latent heat thermal energy storage: Phase change materials, design considerations and performance enhancement techniques”. In: *Renewable and Sustainable Energy Reviews* 27 (2013), pp. 724–737.
- [9] E. Guelpa and V. Verda. “Demand response and other demand side management techniques for district heating: A review”. In: *Energy* 219.119440 (2021).

- [10] E. Hossain et al. “A Comprehensive Review on Energy Storage Systems: Types, Comparison, Current Scenario, Applications, Barriers, and Potential Solutions, Policies, and Future Prospects”. In: *Energies* 13.14 (2020).
- [11] A. Arabkoohsar. *Future Grid-Scale Energy Storage Solutions: Mechanical and Chemical Technologies and Principles*. Department of Civil and Mechanical Engineering, Technical University of Denmark, Lyngby, Denmark, 2023. ISBN: 978-0-323-90786-6.
- [12] A. Sharma et al. “Review on thermal energy storage with phase change materials and applications”. In: *Renewable and Sustainable Energy Reviews* 13.2 (2009), pp. 318–345.
- [13] B. Cárdenas and N. León. “High temperature latent heat thermal energy storage: Phase change materials, design considerations and performance enhancement techniques”. In: *Renewable and Sustainable Energy Reviews* 27 (2013), pp. 724–737.
- [14] T. Nomura, N. Okinaka, and T. Akiyama. “Technology of Latent Heat Storage for High Temperature Application: A Review”. In: *Journal of the Iron and Steel Institute of Japan* 50 (2010), pp. 1229–1239.
- [15] N.V. Khartchenko. *Advanced energy systems*. Taylor Francis Group, LLC, 2010. ISBN: 13: 978-1-4822-1688-2.
- [16] H. Mehling and L. F. Cabeza. *Heat and cold storage with PCM: An up to date introduction into basics and applications*. Springer-Verlag, 2008. ISBN: 978-3-540-68556-2.
- [17] T.M. Letcher. *Storing Energy with Special Reference to Renewable Energy Sources*. University of KwaZulu-Natal, 2016. ISBN: 978-0-12-803440-8.
- [18] A.M. Nair et al. “Phase change materials in building integrated space heating and domestic hot water applications: A review”. In: *Journal of Energy Storage* 54.105227 (2022).
- [19] Z. Khan and Z.A. Khan. “Experimental and numerical investigations of nano-additives enhanced paraffin in a shell-and-tube heat exchanger: A comparative study”. In: *Applied Thermal Engineering* 143 (2018), pp. 777–790.

- [20] R. Jacob and F. Bruno. “Review on shell materials used in the encapsulation of phase change materials for high temperature thermal energy storage”. In: *Renewable and Sustainable Energy Reviews* 48 (2015), pp. 79–87.
- [21] H. Nazir et al. “Recent developments in phase change materials for energy storage applications: A review”. In: *International Journal of Heat and Mass Transfer* 129 (2019), pp. 491–523.
- [22] N.I. Ibrahim et al. “Heat transfer enhancement of phase change materials for thermal energy storage applications: A critical review”. In: *Renewable and Sustainable Energy Reviews* 74 (2017), pp. 26–50.
- [23] M.M. Farid et al. “A review on phase change energy storage: materials and applications”. In: *Energy Conversion and Management* 45 (2004), pp. 1597–1615.
- [24] M. Thonon et al. “Analytical modelling of PCM supercooling including recalescence for complete and partial heating/cooling cycles”. In: *Applied Thermal Engineering* 190.116751 (2021).
- [25] P. Zhang, X. Xiao, and Z.W. Ma. “A review of the composite phase change materials: Fabrication, characterization, mathematical modeling and application to performance enhancement”. In: *Applied Energy* 165 (2016), pp. 472–510.
- [26] A. Sharma et al. “Review on thermal energy storage with phase change materials and applications”. In: *Renewable and Sustainable Energy Reviews* 13.2 (2009), pp. 318–345.
- [27] D. Buddhi and R.L. Sawhney. *Proceedings on thermal energy storage and energy conversion*. Tech. rep. 1994.
- [28] Y. Yuan et al. “Fatty acids as phase change materials: A review”. In: *Renewable and Sustainable Energy Reviews* 29 (2014), pp. 482–498.
- [29] G.A. Lane and D.N. Glew. “Heat of fusion system for solar energy storage”. In: *Proceedings of the workshop on solar energy storage subsystems for the heating and cooling of buildings* (1975), pp. 43–55.
- [30] P. Tan, P. Lindberg, and K. Eichler. “Effect of phase separation and supercooling on the storage capacity in a commercial latent heat thermal energy storage: Experimental cycling of a salt hydrate PCM”. In: *Journal of Energy Storage* 29.101266 (2020).

- [31] T. Xu. “Integrating Latent Heat Storage into Residential Heating Systems”. PhD thesis. KTH Royal Institute of Technology, 2021.
- [32] C. Finck et al. “Quantifying demand flexibility of power-to-heat and thermal energy storage in the control of building heating systems”. In: *Applied Energy* 209 (2018), pp. 409–425.
- [33] R. Hirmiz et al. “Performance of heat pump integrated phase change material thermal storage for electric load shifting in building demand side management”. In: *Energy and Buildings* 190 (2019), pp. 103–118.
- [34] C.P. Underwood et al. “Hybrid thermal storage using coil-encapsulated phase change materials”. In: *Energy and Buildings* 159 (2018), pp. 357–369.
- [35] F.J. Batlles et al. “Development and Results from Application of PCM-Based Storage Tanks in a Solar Thermal Comfort System of an Institutional Building—A Case Study”. In: *Energies* 13.15 (2020).
- [36] Z. Wang et al. “Investigation on the feasibility and performance of transcritical CO₂ heat pump integrated with thermal energy storage for space heating”. In: *Renewable Energy* 134 (2019), pp. 496–508.
- [37] N.J. Kelly, P.G. Tuohy, and A.D. Hawkes. “Performance assessment of tariff-based air source heat pump load shifting in a UK detached dwelling featuring phase change-enhanced buffering”. In: *Applied Thermal Engineering* 71.2 (2014), :809–820.
- [38] J. Lizana et al. “Energy flexible building through smart demand-side management and latent heat storage”. In: *Applied Energy* 230 (2018), pp. 471–485.
- [39] Y. Hamada and J. Fukai. “Latent heat thermal energy storage tanks for space heating of buildings: Comparison between calculations and experiments”. In: *Energy Conversion and Management* 46.20 (2005), pp. 3221–3235.
- [40] J. Zhao et al. “Energy-Saving Analysis of Solar Heating System with PCM Storage Tank”. In: *Energies* 11.1 (2018).
- [41] Y. Wang et al. “Performance evaluation approach for solar heat storage systems using phase change material”. In: *Energy and Buildings* 155 (2017), pp. 115–127.

- [42] H. Huang et al. “Improvement of the efficiency of solar thermal energy storage systems by cascading a PCM unit with a water tank”. In: *Journal of Cleaner Production* 245.118864 (2020).
- [43] Y. Li et al. “Optimal design of PCM thermal storage tank and its application for winter available open-air swimming pool”. In: *Applied Energy* 209 (2018), pp. 224–235.
- [44] J.P. da Cunha and P. Eames. “Compact latent heat storage decarbonisation potential for domestic hot water and space heating applications in the UK”. In: *Applied Thermal Engineering* 134 (2018), pp. 396–406.
- [45] Y. Li, Z. Ding, and Y. Du. “Techno-economic optimization of open-air swimming pool heating system with PCM storage tank for winter applications”. In: *Renewable Energy* 150 (2020), pp. 878–890.
- [46] F. Agyenim and N. Hewitt. “Experimental investigation and improvement in heat transfer of paraffin PCM RT58 storage system to take advantage of low peak tariff rates for heat pump applications”. In: *International Journal of Low-Carbon Technologies* 8.4 (2013), pp. 260–270.
- [47] M.M. Prieto, I. Suárez, and B. González. “Analysis of the thermal performance of flat plate PCM heat exchangers for heating systems”. In: *Applied Thermal Engineering* 116 (2017), pp. 11–23.
- [48] F. Bentivoglio et al. “Design and operation of a 180 kWh PCM heat storage at the Flaubert substation of the Grenoble urban heating network”. In: *Applied Thermal Engineering* 185.116402 (2021).
- [49] F. Agyenim, P. Eames, and M. Smyth. “Heat transfer enhancement in medium temperature thermal energy storage system using a multitube heat transfer array”. In: *Renewable Energy* 35.1 (2010), pp. 198–207.
- [50] A. Agarwal and R.M. Sarviya. “An experimental investigation of shell and tube latent heat storage for solar dryer using paraffin wax as heat storage material”. In: *Engineering Science and Technology, an International Journal* 19.1 (2016), pp. 619–631.
- [51] A.M. Abdulateef et al. “Geometric and design parameters of fins employed for enhancing thermal energy storage systems: a review”. In: *Renewable and Sustainable Energy Reviews* 82.1 (2018), pp. 1620–1635.

- [52] I.S. Chatroudi et al. *Heat transfer enhancement and free convection assessment in a double-tube latent heat storage unit equipped with optimally spaced circular fins: Evaluation of the melting process*. URL: <https://doi.org/10.3389/fenrg.2023.1097382>. (accessed: 2024).
- [53] R. Karami and B. Kamkari. “Experimental investigation of the effect of perforated fins on thermal performance enhancement of vertical shell and tube latent heat energy storage systems”. In: *Energy Conversion and Management* 210.112679 (2020).
- [54] A. Sciacovelli, F. Gagliardi, and V. Verda. “Maximization of performance of a PCM latent heat storage system with innovative fins”. In: *Applied Energy* 137 (2015), pp. 707–715.
- [55] A.M. Abdulateef et al. “Geometric and design parameters of fins employed for enhancing thermal energy storage systems: a review”. In: *Renewable and Sustainable Energy Reviews* 82.1 (2018), pp. 1620–1635.
- [56] S. Zhang, S. Mancin, and L. Pu. “A review and prospective of fin design to improve heat transfer performance of latent thermal energy storage”. In: *Journal of Energy Storage* 62.106825 (2023).
- [57] G.R.Solomon and R. Velraj. “Analysis of the heat transfer mechanisms during energy storage in a Phase Change Material filled vertical finned cylindrical unit for free cooling application”. In: *Energy Conversion and Management* 75 (2013), pp. 466–473.
- [58] Y. Yuan et al. “Effect of installation angle of fins on melting characteristics of annular unit for latent heat thermal energy storage”. In: *Solar Energy* 136 (2016), pp. 365–378.
- [59] A.A. Al-Abidi et al. “Internal and external fin heat transfer enhancement technique for latent heat thermal energy storage in triplex tube heat exchangers”. In: *Applied Thermal Engineering* 53.1 (2013), pp. 147–156.
- [60] M.K. Rathod and J. Banerjee. “Thermal performance enhancement of shell and tube Latent Heat Storage Unit using longitudinal fins”. In: *Applied Thermal Engineering* 75.22 (2015), pp. 1084–1092.
- [61] S. Paria et al. “Performance evaluation of latent heat energy storage in horizontal shell-and-finned tube for solar application”. In: *Journal of Thermal Analysis and Calorimetry* 123.2 (2016), pp. 1371–1381.

- [62] A.H. Mosaffa et al. “Analytical modeling of PCM solidification in a shell and tube finned thermal storage for air conditioning systems”. In: *Energy and Buildings* 49 (2012), pp. 356–361.
- [63] Y. Kozak, T. Rozenfeld, and G. Ziskind. “Close-contact melting in vertical annular enclosures with a non-isothermal base: Theoretical modeling and application to thermal storage”. In: *International Journal of Heat and Mass Transfer* 72 (2014), pp. 114–127.
- [64] R.P. Singh et al. “Effective utilization of natural convection via novel fin design influence of enhanced viscosity due to carbon nano-particles in a solar cooling thermal storage system”. In: *Solar Energy* 183 (2019), pp. 105–119.
- [65] L. Kalapala and J. K. Devanuri. “Effect of orientation on thermal performance of a latent heat storage system equipped with annular fins – An experimental and numerical investigation”. In: *Applied Thermal Engineering* 183.116244 (2021).
- [66] A. Rozenfeld et al. “Experimental demonstration, modeling and analysis of a novel latent-heat thermal energy storage unit with a helical fin”. In: *International Journal of Heat and Mass Transfer* 110 (2017), pp. 692–709.
- [67] S. Zhang et al. “Melting performance analysis of phase change materials in different finned thermal energy storage”. In: *Applied Thermal Engineering* 176.115425 (2020).
- [68] A. Caron-Soupart et al. “Performance analysis of thermal energy storage systems using phase change material”. In: *Applied Thermal Engineering* 98 (2016), pp. 1286–1296.
- [69] A. Sciacovelli and V. Verda. “Second-law design of a latent heat thermal energy storage with branched fins”. In: *International Journal of Numerical Methods for Heat Fluid Flow* 26.2 (2016), pp. 489–503.
- [70] M. Sheikholeslami, S. Lohrasbi, and D.D. Ganji. “Response surface method optimization of innovative fin structure for expediting discharging process in latent heat thermal energy storage system containing nano-enhanced phase change material”. In: *Journal of the Taiwan Institute of Chemical Engineers* 67 (2016), pp. 115–125.

- [71] A.M. Abdulateef et al. “Comparison of pinned and finned tubes in a phase change thermal energy storage system using CFD”. In: *Applied Energy* 104 (2013), pp. 79–86.
- [72] A. Pizzolato et al. “Topology optimization for heat transfer enhancement in Latent Heat Thermal Energy Storage”. In: *International Journal of Heat and Mass Transfer* 104 (2013), pp. 79–86.
- [73] V.R. Voller. “An overview of numerical methods for solving phase change problems”. In: *Advances in Numerical Heat Transfer* 1.9 (1997), pp. 341–380.
- [74] H. Hu and S. A. Argyropoulos. “Mathematical modelling of solidification and melting: a review”. In: *Modelling and Simulation in Materials Science and Engineering* 4.371 (1996).
- [75] J. Stefan. “Über einige Probleme der Theorie der Wärmeleitung”. In: *S-B Wien Akad. Mat. Natur.* 98 (1889), pp. 473–84, 965–83.
- [76] F. Neumannn. In: *Die Paruellen Differentialgleichungen der Mathematischen Physik vol 2* (1912), p. 121.
- [77] H.T. Hashemi and C.M. Sliepcevich. “A numerical method for solving two-dimensional problems of heat conduction with change of phase”. In: *Chem. Eng. Prog. Symp. Series* 63 (1967), pp. 34–41.
- [78] D. Poirier and M. Salcudean. “On numerical methods used in mathematical modeling of phase change in liquid metals”. In: *ASME J. Heat Transfer* 110.3 (1988), pp. 562–570.
- [79] V.R. Voller and L. Shadabi. “Enthalpy methods for tracking a phase change boundary in two dimensions”. In: *International Communications in Heat and Mass Transfer* 11.3 (1984), pp. 239–249.
- [80] M. Iten, S. Liu, and A. Shukla. “Experimental validation of an air-PCM storage unit comparing the effective heat capacity and enthalpy methods through CFD simulations”. In: *Energy* 155.15 (2018), pp. 495–503.
- [81] European Association for Storage of Energy (EASE) and European Energy Research Alliance (EERA). *European energy storage technology development roadmap 2017 update*. Tech. rep. 2017.

- [82] T. Xu et al. “Latent heat storage integration into heat pump based heating systems for energy-efficient load shifting”. In: *Energy Conversion and Management* 236.114042 (2021).
- [83] D. Laing et al. “Development of high temperature phase-change-material storages”. In: *Applied Energy* 109 (2013), pp. 497–504.
- [84] E. Guelpa and V. Verda. “Thermal energy storage in district heating and cooling systems: A review”. In: *Applied Energy* 252.113474 (2019).
- [85] B. He et al. “Designing Paraffin Waxes Phase Change Material (PCM) Cool Storage System for Peak Shaving in District Cooling Systems”. In: 2003.
- [86] B. He. “High-Capacity Cool Thermal Energy Storage for Peak Shaving - A Solution for Energy Challenges in the 21st Century”. PhD thesis. KTH Royal Institute of Technology, 2004.
- [87] A. Pizzolato et al. “Design of effective fins for fast PCM melting and solidification in shell-and-tube latent heat thermal energy storage through topology optimization”. In: *Applied Energy* 208 (2017), pp. 210–227.
- [88] J. Vogel, J. Felbinger, and M. Johnson. “Natural convection in high temperature flat plate latent heat thermal energy storage systems”. In: *Applied Energy* 184 (2016), pp. 184–196.
- [89] J. Vogel and M. Johnson. “Natural convection during melting in vertical finned tube latent thermal energy storage systems”. In: *Applied Energy* 246 (2019), pp. 38–52.
- [90] F. P. Incropera et al. *Fundamentals of heat and mass transfer*. John Wiley Sons, 2007. ISBN: 13: 978-0-471-45728-2.
- [91] A. Micheluz. *Github LHTES repository*. URL: <https://github.com/AlbertoMicheluz/LHTES>. July 2024.

Acknowledgments

I would like to reserve this final section of my thesis for acknowledgments to all those who have contributed, with their invaluable support, to its completion.

First of all, I would like to thank my supervisor Martina for her precious advice and availability. Thank you for guiding me during moments of uncertainty.

Next, I sincerely thank my lifelong friends: Leonardo, Luca, Matteo, and Giovanni. Thank you for lightening these years of study and for always supporting me despite the distance.

I also warmly thank Marta, Giorgia, Elena, and Matteo. Thank you for all the support you have given me and for making these years in Turin unforgettable. The time spent with you is priceless.

Finally, a special thank you goes to my family. To my parents: thank you so much for everything. Thank you for always believing in me; if I have come this far, it is mainly thanks to you. To my brother Leonardo: thank you for all the laughter and good times we shared; your companionship has made this academic journey an unforgettable experience.

Ringraziamenti

Vorrei riservare questo spazio finale della mia tesi di laurea ai ringraziamenti verso tutti coloro che hanno contribuito, con il loro inestimabile supporto, alla realizzazione della stessa.

Per prima cosa, vorrei ringraziare la mia tutor Martina, per i suoi preziosi consigli e per la sua disponibilità. Grazie per avermi saputo indirizzare nei momenti di indecisione.

Ringrazio poi di cuore i miei amici di sempre: Leonardo, Luca, Matteo e Giovanni. Grazie per aver alleggerito questi anni di studio e per avermi sempre sostenuto nonostante la distanza.

Ringrazio inoltre con affetto Marta, Giorgia, Elena e Matteo. Grazie per tutto il supporto che mi avete dato e per aver reso questi anni a Torino indimenticabili. Il tempo passato con voi non ha prezzo.

Un ringraziamento speciale va infine alla mia famiglia. Ai miei genitori: grazie mille per tutto. Grazie per aver sempre creduto in me; se sono arrivato fin qua lo devo soprattutto a voi. A mio fratello Leonardo: grazie per tutte le risate e i bei momenti passati insieme, la tua complicità ha reso questo viaggio accademico un'esperienza indimenticabile.